EPRI
Electric Power
Research Institute

Keywords:
Earthquakes
Site characterization
Hazard assessment
Seismic engineering
Seismology
Geotechnical engineering

EPRI TR-102293
Project 3302
Final Report
November 1993

Guidelines for Determining Design Basis Ground Motions

Volume 5: Quantification of Seismic Source Effects

Prepared by
ELECTRIC POWER RESEARCH INSTITUTE
in cooperation with the Joint Contractors
(Southern Electric International, Commonwealth Research Corporation,
and Public Service Corporation of New Jersey),
the Nuclear Management and Resources Council,
the U.S. Department of Energy and Sandia National Laboratories.

EPRI Leadership in Science and Technology

REPORT SUMMARY

Guidelines for Determining Design Basis Ground Motions

Volume 5: Quantification of Seismic Source Effects

Procedures currently used to assess the nature of earthquake ground motion in Eastern North America introduce considerable uncertainty to the design parameters of nuclear power plants and other critical facilities. This report examines that issue in-depth and provides an engineering model and guideline for selecting a site and assessing its seismic suitability.

INTEREST CATEGORIES

Nuclear seismic risk, design, and qualification
Advanced light water reactors
Risk analysis; management and assessment
Nuclear plant life extension

KEYWORDS

Earthquakes
Site characterization
Hazard assessment
Seismic engineering
Seismology
Geotechnical engineering

BACKGROUND Eastern North America has sparse earthquake activity with rare occurrences of large earthquakes; thus, little data exists to empirically quantify the characteristics of ground motions. Procedures currently used to estimate ground motion effects in this region introduce considerable uncertainty into the process of developing seismic designs, either due to the procedure's subjectivity or the lack of physical calibration.

OBJECTIVES To develop generic relations for estimating ground motion appropriate for site screening; to develop a guideline for conducting a thorough site investigation needed to define the seismic design basis.

APPROACH The project team specifically considered ground motions resulting from earthquakes with magnitudes from 5 to 8, fault distances from 0 to 500 km, and frequencies from 1 to 35 Hz. To develop generic ground motion relations for Eastern North America, they used theoretical models calibrated against data from earthquakes throughout North America and the world. In these models, the contributions to ground motion, including its variability, were evaluated using physical representations of earthquake processes. Earthquake processes involve the initial generation of seismic energy or waves at the earthquake fault ("source effects"), followed by the propagation of seismic waves through the earth's crust ("path effects"), and finally the modification of seismic waves as they travel through soils near the earth's surface ("site effects"). The team also collected and analyzed extensive geotechnical data at three reference sites. This information provided the basis for developing a guideline to help assess site suitability.

RESULTS This project resulted in an engineering model for estimating earthquake ground motions in Eastern North America. The model considers a wide range of earthquake sizes and site conditions and may be used directly for site screening purposes.

The work also resulted in a guideline for conducting geotechnical and seismic engineering investigations needed to determine the design basis for a site. This guideline is appropriate for investigating a wide range of site conditions and soil depths within and outside Eastern North America.

EPRI PERSPECTIVE Cost-effective seismic regulation of nuclear power plants requires site-specific definition of seismic ground motions. The development of engineering procedures for estimating earthquake ground motion can thus benefit both operating and future plants. For licensing application, these procedures are needed

to define the safe shutdown earthquake (SSE). The regulatory guidance found in Section 2.5 of the Standard Review Plan (NUREG 0800) is quite limited in scope and does not reflect the current state of knowledge on earthquake phenomena. With no accepted generic procedures in place, utilities constantly face uncertainty associated with site-specific developments and applications. These factors result in seismic design bases that are excessively conservative and/or contribute to licensing delays, regulatory instability, and high utility costs in the licensing process.

In 1988, EPRI completed a seismic hazard model for the central and eastern United States (NP-4726), including a ground motion model (NP-6074). The present work directly complements NP-4726, while replacing and going significantly beyond the results of NP-6074. The engineering ground-motion model can be used for screening potential sites before conducting extensive site investigations. The guideline provides needed background information to conduct an appropriate geotechnical and seismic engineering investigation of a site for licensing purposes. Additional EPRI reports that provide a basis for the current report include: NP-5577, NP-5875, NP-6304, TR-100409, TR-100410, TR-102261, and TR-102262.

This report is presented in five volumes. Essential background, approach and results are given mainly in Volume 1. Volumes 2, 3, and 4 are appendices containing detailed analyses. Volume 5 (licensed material) contains *Quantification of Seismic Source Effects*, which is summarized in Volume 1, Section 4.

PROJECT

RP3302

EPRI Project Manager: J. F. Schneider

Nuclear Power Division

For further information on EPRI research programs, call
EPRI Technical Information Specialists (415) 855-2411.

Guidelines for Determining Design Basis Ground Motions

Volume 5: Quantification of Seismic Source Effects

TR-102293
Research Project 3302

Final Report, November 1993

Prepared by
ELECTRIC POWER RESEARCH INSTITUTE
in cooperation with the Joint Contractors
(Southern Electric International, Commonwealth Research Corporation,
and Public Service Corporation of New Jersey),
the Nuclear Management and Resources Council,
the U.S. Department of Energy and Sandia National Laboratories.

Prepared for
Electric Power Research Institute
3412 Hillview Avenue
Palo Alto, California 94304

EPRI Project Manager
J. F. Schneider

Advanced Reactors Development
Nuclear Power Division

DISCLAIMER OF WARRANTIES AND LIMITATION OF LIABILITIES

ORGANIZATION(S) THAT PREPARED THIS REPORT:
ELECTRIC POWER RESEARCH INSTITUTE

LIST OF COSPONSORS

Early Site Permit Demonstration Program (ESPDP) Participants

Southern Electric International
42 Inverness Center Parkway
Birmingham, AL 25242

Commonwealth Research Corporation
1400 Opus Place
Downers Grove, IL 60515

Public Service Corporation of New Jersey
80 Park Plaza, 11-A
Newark, NJ 07101

Electric Power Research Institute
3412 Hillview Ave.
Palo Alto, CA 94303

Nuclear Management and Resources Council
1776 Eye Street, Suite 300
Washington, DC 2006

Department of Energy
Office of Nuclear Energy
19901 Germantown, MD 20874

Sandia National Laboratories
1515 Eubank Boulevard Southeast
Albuquerque, NM 87123

PROGRAM PARTICIPANTS

Participants	Affiliation
Project Manager	
Dr. John Schneider	Electric Power Research Institute
Principal Participants	
Dr. Norman Abrahamson	Consultant
Dr. Donald Anderson	CH2M Hill, Inc.
Dr. Gail Atkinson	Consultant
Prof. Carl Costantino	City University of New York
Prof. I.M. Idriss	University of California at Davis
Dr. Robin K. McGuire	Risk Engineering, Inc.
Dr. Robert Nigbor	Agbabian Associates
Dr. Robert Pyke	Consultant
Dr. Walter Silva	Pacific Engineering & Analysis
Dr. Paul Somerville	Woodward-Clyde Consultants—Pasadena
Dr. J. Carl Stepp	Electric Power Research Institute
Prof. Kenneth Stokoe	University of Texas at Austin
Prof. M. Nafi Toksoz	Massachusetts Institute of Technology
Dr. Gabriel Toro	Risk Engineering, Inc.
Dr. Robert Youngs	Geomatrix Consultants
Contributors	
Prof. Keiiti Aki	Consultant
Dr. C. T. Chin	Moh & Associates, Taiwan
Dr. James Chin	University of Southern California
Dr. Shyh-Jeng Chiou	Geomatrix Consultants
Mr. Mark Fuhriman	University of Texas at Austin
Dr. Robert Graves	Woodward-Clyde Consultants
Prof. Robert Herrmann	St. Louis University
Mr. Seon-Keun Hwang	University of Texas at Austin
Mr. Athar Khwaja	University of Texas at Austin
Mr. Joseph Laird	University of Texas at Austin
Mr. David Lapp	Geomatrix Consultants
Mr. Ben T. Lin	Moh & Associates, Taiwan
Mr. Mihalis Madianos	Geomatrix Consultants

Contributors

Dr. Batakrishna Mandal	Massachusetts Institute of Technology
Mr. James McLaren	Woodward-Clyde Consultants
Mr. Bruce Redpath	Redpath Geophysics
Ms. Nancy Smith	Woodward-Clyde Consultants
Ms. Cathy Stark	Pacific Engineering & Analysis
Mr. Robert Steller	Agbabian Associates
Dr. Joseph Sun	Woodward-Clyde Consultants
Dr. Y. T. Gu	City University of New York
Mr. Ernest Heymsfield	City University of New York
Dr. Xiao-ming Tang	Massachusetts Institute of Technology
Mr. Chris Volksen	University of California at Davis
Mr. Donald Wells	Geomatrix Consultants
Mr. Doug Wright	Pacific Engineering & Analysis
Dr. Shen-Chyun Wu	Risk Engineering, Inc.
Ms. Joanne Yoshimura	Consultant

LIST OF CONTRACTORS

Guidelines for Determining Design Basis Ground Motions

TR-102293

Contract	Contractor
RP3302-02	Professor M. Nafi Toksoz Consultant 15 Walsingham St. Newton, MA 02162
RP3302-04	Professor Kenneth Stokoe Consultant 4602 Laurel Canyon Dr. Austin, TX 78731
RP3302-05	Professor I.M. Idriss Consultant P.O. Box 330 Davis, CA 95617-0330
RP3302-06	Dr. Gail Atkinson Consultant 125 Dunbar Road South Waterloo, Ontario N2L 2E8 CANADA
RP3302-07	Dr. Norman Abrahamson Consultant 5319 Camino Alta Mora Castro Valley, CA 94546

Contract	Contractor
RP3302-08	Dr. Paul Somerville Woodward-Clyde Consultants 566 El Dorado St. Pasadena, CA 91101
RP3302-09	Dr. Robin K. McGuire Risk Engineering, Inc. 5255 Pine Ridge Road Golden, CO 80403
RP3302-10	Dr. Walter Silva Pacific Engineering and Analysis 311 Pomona Avenue El Cerrito, CA 94530
RP3302-11	Dr. Robert Pyke Consultant 1076 Carol Lane #136 Lafayette, CA 94549
RP3302-12	Dr. Robert Youngs Geomatrix Consultants 100 Pine Street—10th Floor San Francisco, CA 94111
RP3302-13	Dr. Donald Anderson CH2M Hill, Inc. P.O. Box 91500 Bellevue, WA 98009-2050
RP3302-14	Professor Keiiti Aki Consultant 622 Paseo de la Playa Redondo Beach, CA 90277
RP3302-15	Dr. Joseph Sun Woodward-Clyde Consultants 500 12th Street, Suite 100 Oakland, CA 94607-4014
RP3302-16	Dr. Robert Nigbor Agbabian Associates 1111 South Arroyo Parkway Suite 405 Pasadena, CA 91105
RP3302-18	Prof. Carl Costantino Consultant 4 Rockingham Rd. Spring Valley, NY 10977

ABSTRACT

This report develops and applies a method for estimating strong earthquake ground motion. The emphasis of this study is on ground motion estimation in Eastern North America (east of the Rocky Mountains), with particular emphasis on the Eastern United States and southeastern Canada. Specifically considered are ground motions resulting from earthquakes with magnitudes from 5 to 8, fault distances from 0 to 500 km, and frequencies from 1 to 35 Hz. The two main objectives were: (1) to develop generic relations for estimating ground motion appropriate for site screening; and (2) to develop a guideline for conducting a thorough site investigation needed to define the seismic design basis. For the first objective, an engineering model was developed to predict the expected ground motion on rock sites, with an additional set of amplification factors to account for the response of the soil column over rock at soil sites. The results incorporate best estimates of ground motion as well as the randomness and uncertainty associated with those estimates. For the second objective, guidelines were developed for gathering geotechnical information at a site and using this information in calculating site response. As a part of this development, an extensive set of geotechnical and seismic investigations was conducted at three reference sites. Together, the engineering model and guidelines provide the means to select and assess the seismic suitability of a site.

ACKNOWLEDGMENTS

This project was made possible through extensive support from a great number of institutions and individuals.

For review of draft copies of the report, conducted under an extremely tight schedule, we much appreciate the thoughtful comments by the following individuals: Dr. Michael Bohn, Sandia National Laboratory; Prof. Ricardo Dobry, Rensselaer Polytechnic Institute; Mr. Jeff Kimball, Department of Energy; Dr. Takeji Kokusho, Central Research Institute of Electric Power Industry, Japan; and Dr. Scott Slezak, Sandia National Laboratory.

Field measurements at the reference sites at Treasure Island and Gilroy 2 in California and at Lotung, Taiwan, required considerable logistical coordination and cooperation between institutions and individuals. Major contributions to seismic and other geophysical measurements at Treasure Island and Gilroy 2 were made by Mr. Takashi Kanamori and Mr. Finn Michelson of Oyo Geospace, Mr. Kenji Tanaka of Oyo Corporation, and Mr. Ed Steller of Agbabian Associates. Extensive seismic measurements at Treasure Island and Gilroy 2 were also made by Dr. Ronald Andrus, Mr. Marwan Aouad, and Mr. James Bay of the University of Texas at Austin. Generous support from Mr. Thomas Fumal and Mr. James Gibbs of the U.S. Geological Survey is also acknowledged for their contribution to geologic and seismic logging, respectively, of boreholes at the Gilroy 2 and Treasure Island sites. The following companies assisted the project by providing special equipment used in the measurements: ANCO Engineers, Kinemetrics, Inc., Oyo Corporation, and Redpath Geophysics.

For making arrangements or generously providing access to the reference sites, we are grateful to numerous individuals. We thank Ms. Susan Chang and Dr. Lelio Mejia of Woodward-Clyde Associates for assistance in logistics of drilling at Gilroy 2. Special thanks to Mr. Richard Lake and Mr. Roger Kostenko of Pitcher Drilling Co. for their excellence in drilling and sampling at the Gilroy 2 and Treasure Island sites. Drilling at Lotung, Taiwan, was coordinated expertly by Moh & Associates. We thank Mr. Y. H. Cheng, Deputy Director of the Nuclear Engineering Department at Taiwan Power Co., for helping with access to drilling at the Lotung site owned by Taiwan Power Co. For access to Gilroy 2, we thank Mr. John Belleau, site owner, and Mr. Roger and Ms. Marie Ellissondo, site managers (National 9 Inn). For Treasure Island site access, we thank Mr. Thomas Cuckler and Mr. Donald Brown of the Civil Engineering Department of the Treasure Island Naval Air Station.

Additional data were also generously provided by many individuals and institutions from complementary field measurements at various field test sites. Prof. Pedro de Alba of the University of New Hampshire, Mr. John Egan of Geomatrix Consultants, Prof. Roman Hryciw of the University of Michigan, and Prof. Kyle Rollins of Brigham Young University all generously provided data for our use from other geotechnical studies at Treasure Island. Sponsors of studies that produced these data were the U.S. Naval Air Station and the National Science Foundation. Prof. Pedro de Alba also provided access to boreholes drilled for several of these studies, also sponsored by the National

Science Foundation. Mr. Jeff Kimball of the Department of Energy made it possible to use a collection of geotechnical data from a site at the Savannah River site, South Carolina.

All of the laboratory measurements of dynamic properties of soil samples from the reference sites were performed at the Geotechnical Engineering Center of the University of Texas at Austin (GEC-UT). The large-scale chamber tests used to study field damping measurements were also performed at the GEC-UT. We thank Mr. Ngarkok Lee and Mr. Mark Twede of that institution for their assistance in this work. Further, the assistance of Ms. Teresa Tice-Boggs of the Geotechnical Engineering Center contributed significantly to the success of this work.

Several people assisted in providing and assembling data for the earthquake database used in this project. We appreciate the help of Mr. Phillip Munro of the Geological Survey of Canada for information regarding characteristics of strong-motion instrument sites for data recorded during the 1988 Saguenay, Quebec, earthquake and aftershocks.

Dr. David Boore of the U. S. Geological Survey provided an analysis of the distribution of selected ground motion data recorded on Wood-Anderson seismographs in southern California. Dr. Gail Atkinson provided seismic data and site descriptions from the Eastern Canada Telemetered Seismic Network.

We would like to thank the following people for their participation in various workshops held during the course of the project: Dr. David Boore, Dr. Jon Fletcher, Mr. Thomas Fumal, Mr. James Gibbs, Dr. William Joyner, and Dr. John Vidale of the U.S. Geological Survey; Mr. Scott Ashford, University of California at Berkeley; Ms. Ornella Bonamassa, University of California at Santa Cruz; Dr. David Rodgers, Rogers Pacific Consultants; Mr. Takashi Kanamori and Mr. Finn Michelson of Oyo Geospace; Dr. Clifford Roblee, California Department of Transportation; and Dr. Richard Lee, Westinghouse Savannah River Co. These individuals participated in numerous stimulating discussions that greatly contributed to the final product.

Finally, it is with great appreciation for the financial and managerial support, and, equally important the trust and confidence provided us, that we thank various individuals within and associated with the Department of Energy and utility industry for making the project possible. Special thanks to Ms. Susan Gray, Mr. Murv Little, and Mr. Joseph Santucci of the EPRI Advanced Reactor Program for their generous support, and especially to Ms. Gray for her direction as project manager of the Early Site Permit Demonstration Program. Thanks to Mr. Walter Pasedag of the Department of Energy and Mr. Ajoy Moonka of Sandia National Laboratory; to the Industry Siting Group, especially Mr. Louis Long; to the Nuclear Management and Resources Council (NUMARC), especially Mr. John Ronafalvy; to the Joint Contractors comprised of Southern Electric International, Commonwealth Research Corporation, and Public Service Company of New Jersey, especially Dr. Ninu Kaushal (Commonwealth Edison Co.).

CONTENTS

Volume 5: Quantification of Seismic Source Effects

LIST OF FIGURES

Figures **Page**

LIST OF TABLES

Figures **Page**

EXECUTIVE SUMMARY

Introduction

This report develops and applies a method for estimating strong earthquake ground motion. The motivation for this development was the need for a systematic, physically based, empirically calibrated method that can be used to estimate ground motions for input to the design of nuclear power plants and other critical facilities. These ground motions are a function of the earthquake's magnitude and the physical properties of the earth through which the seismic waves travel from the earthquake fault to the site of interest. Procedures currently used to account for these effects introduce considerable uncertainty into the ground motion determination, either due to subjectivity of the procedure or the lack of physical calibration.

The emphasis of this study is on ground motion estimation in Eastern North America (east of the Rocky Mountains), with particular emphasis on the Eastern United States and southeastern Canada. Eastern North America is a stable continental region, having sparse earthquake activity with rare occurrences of large earthquakes. In the absence of large earthquakes within the region of interest, little data exist to empirically quantify the characteristics of ground motions associated with these events. While methods developed in more seismically active areas such as Western North America can be applied to Eastern North America, fundamental differences in the regional geology can lead to variations in ground motion characteristics. Therefore, empirically based approaches that are applicable for other regions, such as Western North America, do not appear to be appropriate for Eastern North America.

Recent advances in science and technology have now made it possible to combine theoretical and empirical methods to develop new procedures and models for estimating ground motion within Eastern North America. Specifically considered are ground motions resulting from earthquakes with magnitudes from 5 to 8, fault distances from 0 to 500 km, and frequencies from 1 to 35 Hz. The results of this report can be used to determine seismic hazards, provided the magnitudes and distances of potential earthquakes are predetermined. In particular, this report is intended for use in site screening as well as detailed characterization of ground motion at a site, such as may be required for structural design.

This study was conducted by a team of experts in seismology, geotechnical engineering, and seismic engineering. The investigations were carried out over a period of approximately 18 months from September 1991 to March 1993. Work included a series of focused workshops with project participants to help achieve consensus recommendations. The project was sponsored by the U. S. Department of Energy (DOE), Sandia National Laboratories, Southern Electric International, Commonwealth Research Corporation, Public Service Company of New Jersey, and the Electric Power Research Institute as part of the DOE's Early Site Permit Demonstration Program. The project was managed by the Electric Power Research Institute.

Objectives

There were two central objectives of the project: (1) to develop generic relations for estimating ground motion

appropriate for site screening; and (2) to develop a guideline for conducting a thorough site investigation needed to define the seismic design basis. For the first objective, a set of relations was needed that could be used to predict the expected ground motion on rock or on soil for a future earthquake. The approach was to develop an engineering model consisting of relations appropriate for rock sites and an additional set of amplification factors to account for the response of the soil column over rock at soil sites. For the second objective, a guideline was developed for gathering geotechnical information at a site and using this information in calculating site response. Together, the engineering model and guideline provide the means to select and assess the seismic suitability of a site.

Approach

The method that was used to develop generic ground motion relations in this effort is markedly different from the approach of previous studies. In this study, theoretical models, which have been calibrated against data from earthquakes throughout North America and the world, are used to characterize earthquake ground motion in Eastern North America. In these models, the contributions to ground motion, including its variability, are evaluated using physical representations of earthquake processes. These processes involve the initial generation of seismic energy or waves at the earthquake fault ("source effects"), followed by the propagation of seismic waves through the earth's crust ("path effects"), and finally the modification of seismic waves as they travel through soils near the earth's surface ("site effects"). For a given earthquake magnitude and distance, the source, path, and site each contribute to the observed ground motion, as follows:

- The source controls both the seismic energy generated by rupture of an earthquake fault as well as the accompanying dynamic characteristics.
- The seismic path contributes to ground motion through reflection, refraction, and damping of seismic waves within the earth's crust in response to the various physical properties along the wave path.
- The site contributes to the evolution of seismic waves in much the same way as the path, though on a smaller scale. Site effects are a function primarily of soil depth and type.

The characteristics of the seismic source, path, and site effects form the basis for the parameters in the theoretical models.

The ground motion relations for rock sites were developed using a physically based, empirically calibrated ground motion model. In the model, a wide range of values was assigned to the ground motion parameters. Using the combination of all model parameters and their ranges of values, computer simulations produced hundreds of records of earthquake ground motion for each magnitude and distance considered. While each earthquake simulation represents a possible future earthquake, each earthquake is not equally likely to occur. Therefore, based upon extensive analyses of past earthquakes and comparisons to model predictions, distributions were assigned to the values for all model parameters. The parameter value distributions were based on partitioning their variability into two types: uncertainty, which is due to the lack of knowledge of earthquake characteristics; and randomness, which is due to the inherent variability of those characteristics. Finally, individual parameter weights were combined for each earthquake simulation to produce the appropriate "distribution" of earthquake ground motion for every magnitude, distance, and frequency considered. Together, these distributions constitute a family of functional relations that define the final engineering ground motion model for rock sites. In turn, the engineering model defines ground motion for median levels and associated variability.

To accommodate sites with soil overlying rock (referred to as local site effects), site amplification factors were developed for a range of soil types and depths representative of soil conditions in Eastern North America. The factors were derived by first accumulating data that describe the behavior of various soils during seismic loading. These data were then used to assess the variability in seismic properties, especially the wave velocity as it changes with depth. In addition, seismic velocity and material damping data were gathered from three reference sites using a variety of field and laboratory techniques. The reference site data were used (1) to improve physical understanding of the dynamic processes of soil response and (2) to assess procedures for measuring the physical properties needed to estimate site effects. The estimation problem is particularly difficult because the seismic properties of soils change depending upon the

level of shaking. The resulting "nonlinear" effects generally cause the ratio of soil-to-rock motions (i.e., soil amplification) to decrease as the corresponding rock motion increases. The quantification of these effects through theoretical modeling and comparisons to empirical data resulted in factors that describe the amplification of soils relative to rock for several soil categories. The amplification factors were developed for a wide range of rock motions and are given as median values with variability.

Finally, based upon extensive geotechnical data that were collected at the three reference sites and analyzed as part of this program, a guideline was developed for assessing soil characteristics and site response. This guideline applies to planning and conducting a systematic and thorough geotechnical investigation of soil properties at a potential site. Guidance is also provided for performing dynamic analyses required to determine the response of the soil column to earthquake shaking at (and beyond) the levels of motion of interest to the seismic design.

Conclusions

The engineering ground motion model developed in this study can be used for screening potential sites in Eastern North America before conducting extensive site investigations. However, the application of these procedures to site screening requires information regarding earthquake magnitudes and distances as well as certain site properties such as soil depth and site geology. Magnitudes and distances of potential earthquakes may be derived either probabilistically or deterministically.

The guideline—together with the results of investigations of the three reference sites—provides the means to conduct an appropriate geotechnical and seismic engineering site investigation. In all, this guideline is appropriate for use given a wide range of site conditions and soil depths. While there are certain soil types (e.g., those with liquefaction potential) for which this guideline may not be directly applicable, it may be used widely both within and outside Eastern North America.

The information compiled in this report represents a comprehensive assessment of the nature of earthquake ground motion in Eastern North America. The results incorporate best estimates of ground motion as well as the randomness and uncertainty associated with those estimates for a wide range of earthquake magnitudes, distances, and frequencies. Overall, the results of this study will be useful in performing seismic hazard evaluations and establishing seismic design standards for many years to come.

Organization

The results of this study are presented in five volumes. *Volume I: Methodology and Guidelines for Estimating Earthquake Ground Motion in Eastern North America,* represents the main body of the report, presents the model development and summarizes the key results and conclusions of the study. *Volume II: Appendices for Ground Motion Estimation,* presents the appendices to Sections 2 to 7 of Volume I, and consists primarily of data and details of analyses used to develop the engineering ground motion model and geotechnical guidelines. *Volume III: Appendices for Field Investigations,* and *Volume IV: Appendices for Laboratory Investigations,* present the details of field and laboratory investigations of reference sites; Section 8 of Volume 1 constitutes a summary of these appendices. *Volume V: Seismic Source Effects,* presents separately (as a licensed report) the analyses of the seismic source performed for input to the engineering ground motion model; a summary of this volume is given as Section 4 of Volume 1.

QUANTIFICATION OF SEISMIC SOURCE EFFECTS

There are three main parameters of the seismic source for the stochastic ground motion simulation procedure described in Section 3.2. They are magnitude, stress drop (corner frequency), and the relation between source distance and equivalent point-source distance (accounts for effect of extended sources). This section describes the development of these three parameters.

V.5.1 Magnitude

The m_{Lg} magnitude scale was introduced by Nuttli (1973) as a way to characterize the size of ENA earthquakes using seismograph recordings obtained at regional distances (roughly 100 to 1000 km). m_{Lg} was intended to be consistent with the teleseismic m_b scale, but significant, and often systematic, differences arise between m_b and m_{Lg} magnitudes. m_{Lg} is sometimes denoted as m_{bLg}, m_N, or m_b. The m_{Lg} scale is the magnitude scale most commonly used to characterize the size of contemporary earthquakes in ENA. Macroseismic estimates of earthquake size for pre-instrumental earthquakes (typically in terms of epicentral intensity or felt area) may be converted to m_{Lg} using existing intensity to magnitude relationships (e.g., Herrmann and Nuttli, 1980; EPRI, 1986). These relationships, especially those for intensity, are relatively robust because there are numerous moderate-magnitude ENA events with estimates of both epicentral intensity and m_{Lg}, which have been used to develop these relationships (see EPRI, 1986). Most seismic hazard studies for ENA, such as the recent EPRI/SOG and LLNL seismic hazard studies (EPRI, 1986; LLNL, 1989), have used m_{Lg} to characterize earthquake size.

In addition to developing attenuation equations in terms of m_{Lg}, this study uses the moment magnitude, **M**, (Hanks and Kanamori, 1979) to characterize earthquake size and develops attenuation functions in terms of **M**. **M** is a function of the seismic moment, M_0 (i.e.

$$\mathbf{M} = \frac{2}{3}\log_{10} M_0 - 16.1),$$

which is one of the basic parameters in the ground-motion model developed in this study (see Section 3.2). The use of m_{Lg} provides a link to ENA earthquake catalogs and to current and past practice. The use of **M** provides a more direct and physically based estimate of ground motion.

V.5.1.1 Relationship between m_{Lg} and Seismic Moment

Because earthquake size is characterized by seismic moment M_0 in the ground-motion model of Section 3, one must know the relationship between m_{Lg} and seismic moment (or moment magnitude) in order to develop an attenuation function in terms of m_{Lg}. This relationship may be developed empirically (e.g., Nuttli, 1983; Atkinson, 1984; Somerville, 1986) or by predicting seismogram amplitudes for multiple values of seismic moment, using a ground-motion model such as the stochastic model in Section 3.2 (e.g., Hanks and Boore, 1984; Boore and Atkinson, 1987; Toro and McGuire, 1987). We follow a hybrid approach in this study, using the stochastic ground-motion model in Section 3.2 to develop an average M_0–m_{Lg} relationship. We then use data to validate this relationship and to quantify the variability in m_{Lg} given M_0 and the dependence of m_{Lg} on stress drop.

To obtain the average M_0–m_{Lg} relationship, we use the stochastic ground-motion model described in Section 3.2 and a certain crustal structure to calculate the amplitude of a hypothetical vertical-component short-period WWSSN seismograph (Luh, 1977) at a distance of 500 km[1]. This amplitude, the associated zero-crossing period, and the distance of 500 km are then inserted into Nuttli's equation for m_{Lg} (Nuttli, 1973), obtaining m_{Lg} for a given value of M_0. Repeating this process for multiple values of seismic moment (corresponding to moment magnitudes 4.5 to 8.0), one obtains a relationship between M_0 and m_{Lg}. Performing this operation for all parameter combinations and averaging the results, one obtains an average M_0–m_{Lg} relationship. Only one of the two crustal models to be introduced in Section 5 (i.e. Mid-continent model) is considered in these calculations. It is not necessary to develop separate relationships for the other crustal model (i.e. the Gulf model) because most regional recordings of events from the Gulf region are obtained at stations deep in the Mid-continent region. Therefore, most of the paths for these records lie in the Mid-continent region.

Figure V.5-1 shows the average M_0–m_{Lg} relationship obtained as described above and compares it to the M_0–m_{Lg} data compiled by Boore and Atkinson (1987) and to the relationship obtained by McGuire et al. (1988). Both comparisons indicate good agreement. Additional comparison to the M_0–m_{Lg} data (**M**>5) compiled by Atkinson (1993) shows a bias of 0.05±0.06 and a standard error of 0.25, indicating close agreement (see Figure V.5-2). The average M_0–m_{Lg} relationship may be expressed as a polynomial on **M** as follows

$$m_{Lg}(\text{average}) = -10.23 + 6.105\mathbf{M} - 0.7632\mathbf{M}^2 + 0.03436\mathbf{M}^3 \qquad \text{(Eq. V.5-1)}$$

This curvilinear **M**–m_{Lg} relationship is adopted, even though a linear relationship would also fit the data in Figure V.5-2, because the curvilinear form is a direct consequence of the curvature in the Brune spectral shape in the neighborhood of the corner frequency.

In order to properly calculate the variability in the ground motion predictions in terms of m_{Lg}, it is necessary to investigate the relationship between stress drop and deviations of m_{Lg} from the average values. Modeling results indicate that the effect of stress drop on m_{Lg} is small for moment magnitudes 4 to 5 and increases with increasing seismic moment (see Figure V.5-3). Thus, we investigate the dependence of the quantity

$$\varepsilon = \frac{m_{Lg}(\text{observed}) - m_{Lg}(\text{average})}{\mathbf{M} - 4} \qquad \text{(Eq. V.5-2)}$$

on stress drop, using those events in Atkinson's (1993) data set that have estimates of seismic moment, m_{Lg}, and stress drop. Figure V.5-4 shows ε as a function of stress drop for **M**>5 and suggests a dependence on stress drop which is consistent with modeling results. The one point that deviates significantly from a straight line corresponds to the 1925 Charlevoix earthquake. Because the data for Charlevoix is no less reliable than data from other historical earthquakes, the Charlevoix data are retained and included in a regression analysis to determine the dependence of ε on stress drop, Δσ. This regression yields

$$\varepsilon = 0.16\ (\pm 0.02) + 0.13(\pm 0.08)\ \ln \Delta\sigma + \delta \qquad \text{(Eq. V.5-3)}$$

where δ is a random variable with zero mean and a standard deviation of 0.12. This regression has an R^2 of 0.48, indicating that variability in stress drop given by the regression explains 48% of the variability in ε. The resulting model for m_{Lg} is given by

$$m_{Lg} = m_{Lg}(\text{average}) + (\mathbf{M}\text{-}4)\ (0.16 + 0.13 \ln \Delta\sigma + \delta) \qquad \text{(Eq. V.5-4)}$$

where m_{Lg}(average) is given by the polynomial in Equation V.5-1.

The relationship between m_{Lg} and stress drop affects only the variability in the attenuation equations in terms of m_{Lg} (see Section 9), and has no effect on median ground motion amplitudes. Even though the number of data in Figure V.5-4 and their associated uncertainties do not require a relationship between m_{Lg} and stress drop, the observed effect is consistent with the theoretical dependence shown in Figure V.5-4 and is used in the development of the engineering model in Section 9.

1. The use of a wider-band seismograph response, such as that of a Wood-Anderson, would decrease the calculated m_{Lg} by 0.1 to 0.2 magnitude units; similarly, use of a reference distance of 800 km would decrease the calculated m_{Lg} by 0.1 magnitude units or less (Toro, 1988).

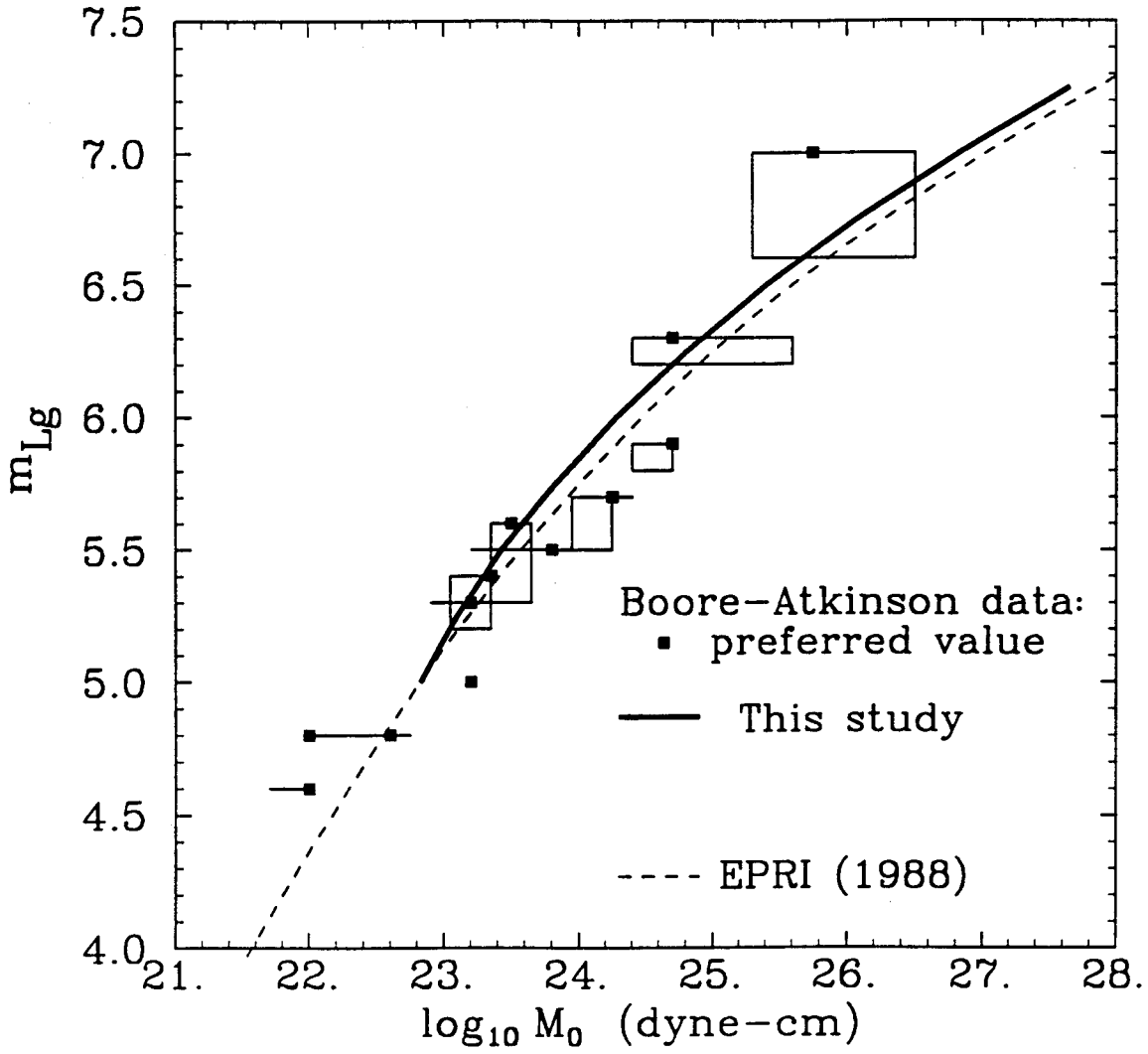

Figure V.5-1. Average predicted M_0–m_{Lg} relationship calculated using the ground-motion model in Section#3 (heavy solid line). Also shown are the relationship obtained by McGuire et al. (1988, dashed line) and the M_0–m_{Lg} data of Boore and Atkinson (1987, rectangles).

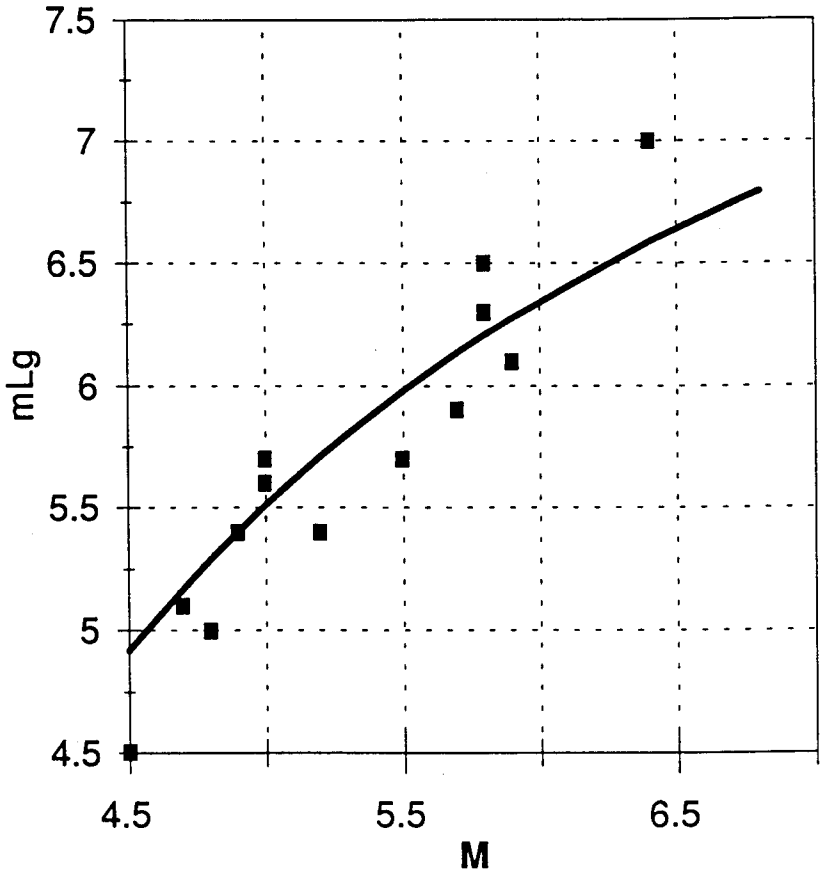

Figure V.5-2. Comparison of the average predicted M_0–m_{Lg} relationship to the data compiled by Atkinson (1993).

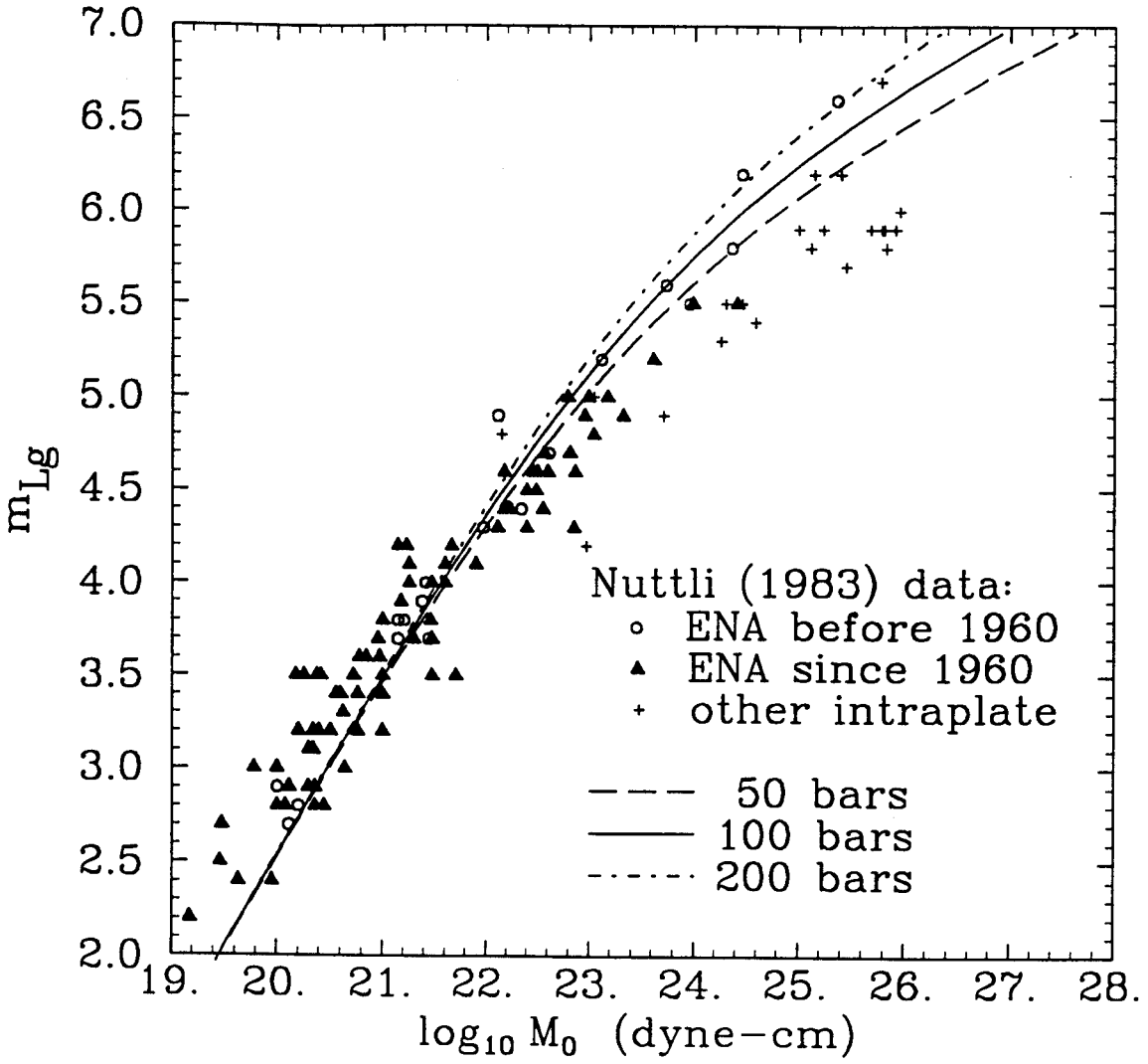

Figure V.5-3. Dependence of the M_0–m_{Lg} relationship on stress drop. Source: McGuire et al. (1988).

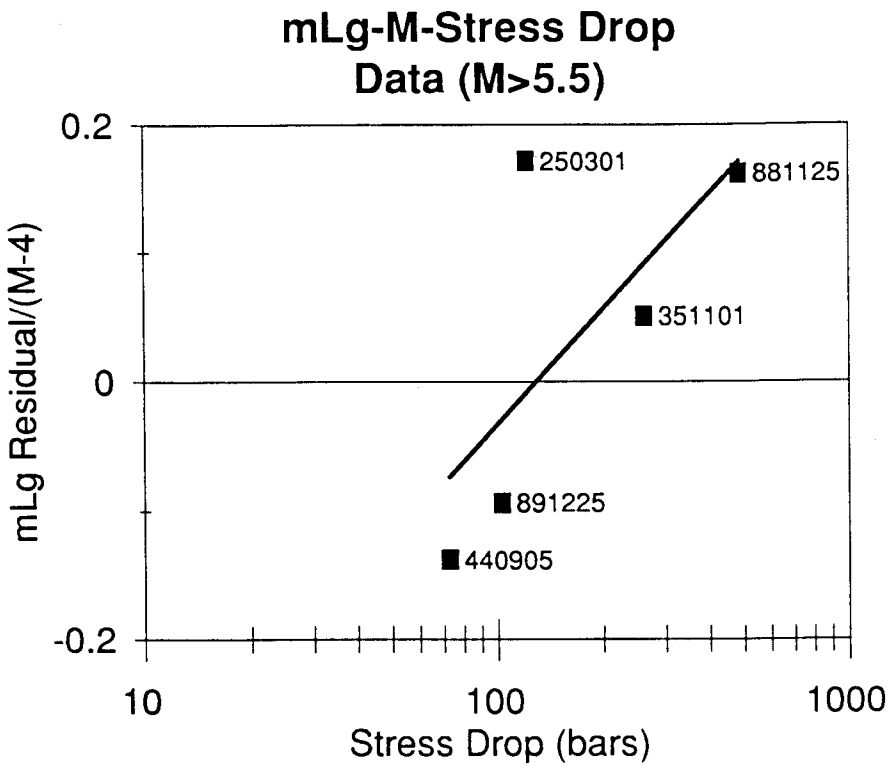

Figure V.5-4 Relationship between m_{Lg} residuals and stress drop. Data from Atkinson (1993).

V.5.1.2 Effect on Ground-Motion Variability

Use of m_{Lg} instead of **M** as the measure of earthquake size results in a moderate decrease in the total variability of the predicted ground motion. This decrease comes about because a higher than average stress drop results in both a higher m_{Lg} and a higher spectral acceleration, thereby increasing the correlation between m_{Lg} and spectral acceleration. The amount of this decrease in variability is magnitude-dependent and is also different for the various ground-motion measures (slight increases occur at some magnitudes for 1 Hz spectral acceleration). Additional discussion of the variability is contained in Section 9.

V.5.2 Stress Drop

For a fixed magnitude or moment, the stress drop in the stochastic source model (Eq. 3.1) directly scales ground motions for frequencies above the corner frequency (Boore, 1983; Silva, 1991). In the frequency range of interest, 1–25 Hz, the stress drop is therefore one of the controlling parameters for the point-source model (Section 9).

For the Brune source model (Section 3.2), the stress drop is computed from the corner frequency. The stress drop is calculated from the moment and corner frequency using the relation

$$\Delta\sigma = 8.44\, M_o \left(\frac{f_c}{\beta_o}\right)^3 \qquad \text{(Eq. V.5-5)}$$

The estimated ΔT depends on the assumed shear wave velocity at the source. For the single corner Brune model, the stress drop is related to the high frequency spectral level for all frequencies above the corner frequency. In contrast, the term stress parameter is used to describe the equivalent stress drop that is derived directly from the high frequency spectral level for frequencies much greater than the corner frequency. The spectral parameter is applicable to models that have more than one corner frequency (Section V.5.2.3).

In this section, two methods are used to estimate the stress drop for EUS earthquakes. The first method is based on the high frequency level of the Fourier amplitude spectrum. The second method is based on fitting the Fourier amplitude over the entire frequency band to the omega-square spectral shape.

V.5.2.1 Estimation of High-Frequency Stress Parameters

High-frequency stress parameters for EUS events were estimated by Atkinson (1993) using both instrumental data and felt areas. The stress parameter values are estimated from the high-frequency spectral level ($f>>f_c$) at the earthquake source (see Eq. 3.1 and 3.3). The source spectral levels were obtained by regression analyses of spectral data for events from 1982 onwards. The high frequency source spectral levels for older events were estimated based on MMI data using the Atkinson (1993) relation between felt area of ENA earthquakes and their high frequency levels at the source. She found that the stress parameters for aftershocks were significantly smaller than for mainshocks. Therefore, aftershocks are not included in the current study. The Atkinson stress parameters were modified to be consistent with the shear-wave velocity values in the focal region for the Mid-continent crustal model (Section 5) based on Eq. V.5-5. The "equivalent Mid-continent stress parameters" are listed in Table V.5-1. The modification is required

Table V.5-1

High-Frequency Stress Parameters for EUS Events Based on the Mid-continent Crustal Velocities

Date	Name	M	Equivalent Mid-continent Stress Parameter (bars)
25-03-01	Charlevoix	6.4	122
29-11-18	Grand Banks	6.7	90
35-11-01	Timiskaming	5.8	261
39-10-19	Charlevoix	5.3	90
40-12-20	Ossippee	5.5	70
44-09-05	Cornwall	5.7	73
68-11-09	S. Illinois	5.38	456
80-08-27	Sharpsburg	5.05	217
82-01-09	Miramichi AS	5.5	53
82-01-19	New Hampshire	4	59
83-10-07	Goodnow	5	78
85-10-05	Nahanni FS	6.7	61
85-12-23	Nahanni MS	6.8	37
86-01-31	Painesville	4.8	103
86-07-12	Ohio	4.5	106
87-06-10	Illinois	4.96	122
88-11-23	Sag FS	4.1	179
88-11-25	Sag MS	5.8	488
89-03-16	Payne Bay	5	183
89-12-25	Ungava	5.9	103
90-10-19	Mont Laurier	4.7	357

because Atkinson assumed a shear wave velocity at the source that is different from the Mid-continent model used in the study. For example, at a depth of 10 km Atkinson used a shear wave velocity of 3.8 km/s, whereas the Mid-continent model has 3.5 km/s. To account for this difference, Atkinson's stress parameter for this focal depth is divided by the factor $(3.8^3/3.5^3)^{1.5}$ which is about 1.45. With this modification, these stress parameters can be used in the stochastic model with the Mid-continent velocity structure to yield high frequency spectral levels that are consistent with the empirical data base.

These high frequency stress parameters are plotted versus moment magnitude in Figure V.5-5. These data show a decrease of stress parameter for magnitudes greater than 6.0; however, a linear least-squares fit of log stress parameter versus magnitude is not statistically significant at the 95% confidence level. The stress parameters range from 37 to 488 bars. The mean natural log stress parameter is 4.79±0.16 (120 bars) with a standard error of a single observation of 0.71 on the natural logarithm of stress parameter.

V.5.2.2 Estimation of Brune Stress Drops

Brune stress drops may be estimated either in the time domain, by measuring the source duration and seismic moment, or in the frequency domain by measuring corner frequency and seismic moment. In a previous study sponsored by EPRI, Somerville et al. (1987) used the time domain approach to estimate median stress drops of 120 bars and 90 bars for large earthquakes in eastern and western North America respectively based on teleseismic data. Comparable values have been estimated in the present study by fitting the Fourier amplitude spectrum of near-source recordings to the omega-square spectral model given in Equation 3.1. The methodology, described below, was applied to both stable continental interiors and tectonically active regions.

V.5.2.2.1 Methodology

In the inversion scheme, earthquake source, path, and site parameters are obtained by using a nonlinear least-squares inversion of Fourier amplitude spectra for the stochastic model parameters in Equation 3.1 (Silva and Stark, 1992). The bandwidth for each amplitude

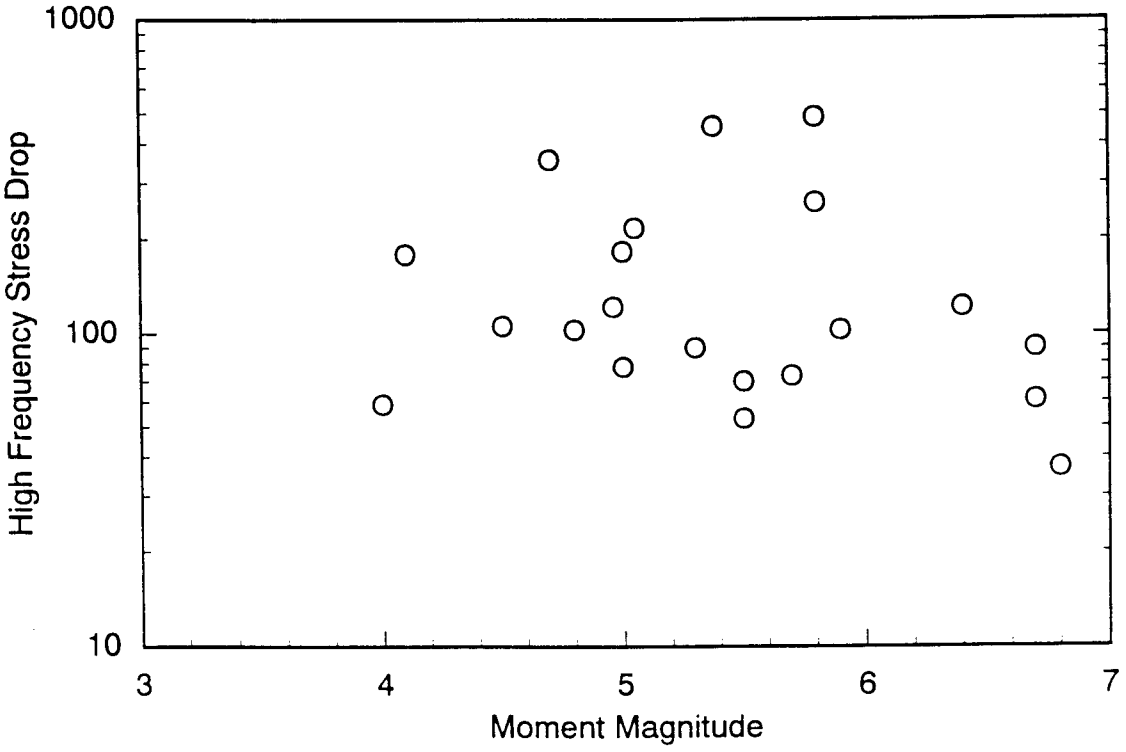

Figure V.5-5. High-frequency stress parameters modified from Atkinson (1993) to be consistent with the Mid-continent velocity structure.

spectrum computed from recordings was selected based upon visual examination. In no case did the bandwidth extend beyond either instrument or filter corner frequencies. For horizontal components the vector sum amplitude spectrum divided by $\sqrt{2}$ is used. This tends to minimize the effects of resonances and results in more stable inversions. Generally, when source to site distances exceeded about 50 km, the effects of crustal structure (Ou and Herrmann, 1990) were incorporated in the inversion. For all the cases considered, however, the resulting inversions were not measurably improved by using crustal structure effects: there was little or no reduction in the standard error of the fit. In some cases, the fit was actually degraded. Consequently, results are presented for inversions using only the simple geometric attenuation terms.

The inversion scheme treats multiple earthquakes and sites simultaneously with a common crustal path damping parameter Q(f). In total, six parameters may be determined depending upon the number of stations per earthquake and distance ranges. The parameter covariance matrix is examined to determine which parameters may be resolved for each data set. In the stochastic ground motion model (Section 3.2), the six parameters which may be determined include: kappa (frequency-dependent site-specific attenuation), D (frequency-independent site-specific amplification), Q_0 and η (frequency-dependent path Q model), **M**, and corner frequency (Silva and Stark, 1992). The constant term D allows broad-band adjustment of the modeled spectrum at each site. Crustal and soil profile amplification is accommodated in the inversion scheme by incorporating the appropriate transfer functions in the model spectra.

To reduce the non-uniqueness inherent in inversion schemes, a suite of starting models is employed. The final set of parameters is selected based upon a visual inspection of the model fit to the Fourier amplitude spectrum as well as the chi-square values. In this approach, a consistent method which accommodates path Q(f) as well as kappa and crustal amplification is used.

V.5.2.2.2 Brune Stress Drops for Stable Continental Regions

For applications to eastern North America, 12 earthquakes were studied with magnitude greater than or equal to 4.0, which occurred in what is considered the

Table V.5-2

Brune Stress Drops for SCR Events

Date	Time	Name	M	N	$\Delta\sigma$	SE ($\Delta\sigma$)
82-01-11		New Brunswick (A)	5.0	9	132	86
82-01-19		New Hampshire	4.0	4	66	16
82-03-31		New Brunswick (A)	4.2	9	96	5
82-06-16		New Brunswick (A)	4.2	5	100	21
83-10-07		Goodnow, New York	5.0*	6	269	39
85-12-23	05:16	Nahanni, NW Terr.	6.8*	3	86	4
85-12-23	05:48	Nahanni, NW Terr. (A)	5.4*	1	91	4
88-11-23		Saguenay, Quebec	4.0	6	53	20
88-11-25		Saguenay, Quebec	5.8*	11	655	32
89-04-27		Missouri	4.2	2	229	120
90-10-19		Montlaurier, Quebec	4.5	12	437	64
91-05-04		Cape Girardeau, Miss.	4.4	4	39	31

* Magnitude fixed in inversion
(A) designates aftershock

North American Stable Continental Region. Results of the inversions are shown in Table V.5-2 for each earthquake. Magnitudes ranged from 4.0 to 6.8. The computed stress drops range from 39 bars to 655 bars. The mean natural log stress drop is 4.86±0.25 (130 bars) with a standard error of a single observation of 0.86 on the natural logarithm of $\Delta\sigma$. The stress drops are shown as a function of magnitude in Figure V.5-6. This data set does not indicate a magnitude dependence of stress drop. Four of the 12 events are aftershocks. The mean natural log stress drop for the 8 mainshocks is 4.98±0.37 (145 bars). Due to the small sample size, the mean log stress drop for this data set (4.98±0.37) is not significantly different from the mean log stress parameter for the larger Atkinson data set (4.79±0.16).

V.5.2.2.3 Brune Stress Drops for Tectonically Active Regions

For comparison, the Brune stress drops were computed for tectonically active regions using the same inversion procedure. A total of 25 mainshocks with magnitudes greater than or equal to 4.0 were studied. The source regions include California, the Basin and Range province, Italy, and the 1978 Tabas, Iran earthquake. Distances were generally within 100 km and all inversions were performed using the 1/R geometrical attenuation term. Results of the inversions are shown in Table V.5-3 for each earthquake. The median stress drop is 100 bars with a standard error of 0.68 on the natural logarithm of stress drop. The stress drops are plotted as a function

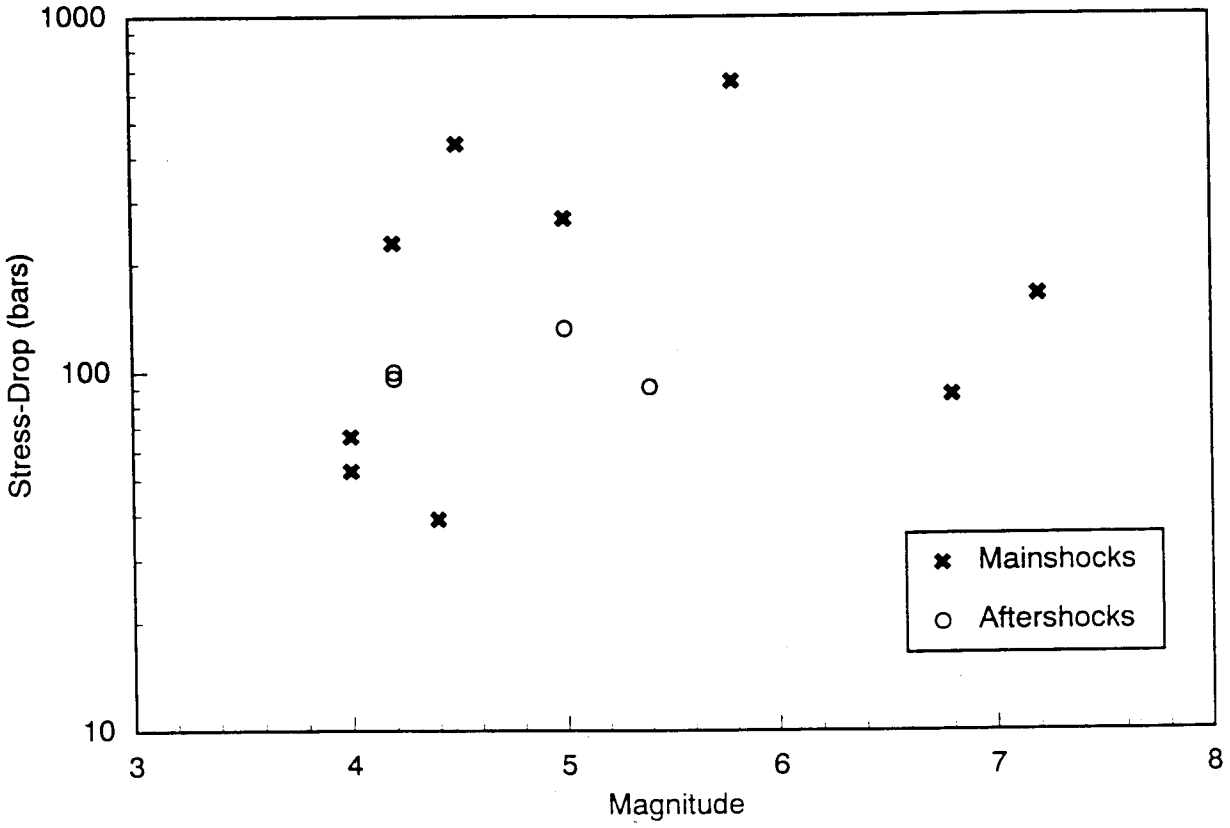

Figure V.5-6. Brune stress-drops for SCR estimated by inversion of the Fourier amplitude spectrum.

Table V.5-3

Brune Stress Drops for Active Regions Events

Date	Time	Name	M	N	$\Delta\sigma$	SE ($\Delta\sigma$)
33-03-11		Long Beach	6.4*	3	112	11
35-10-31		Montana	6.1	1	49	77
35-11-28		Montana	5.1	1	102	52
40-05-19		Imperial Valley	6.9*	1	86	13
52-07-21		Kern County	7.5*	4	186	35
57-03-22		San Francisco	5.3	5	114	44
62-08-30		Cache Valley	5.9*	1	28	6
66-06-28		Parkfield	6.3	5	154	94
68-04-09		Borrego Mtn.	6.6*	2	108	34
70-09-12		Lytle Creek	5.3	3	108	37
71-02-09		San Fernando	6.6*	9	52	13
76-05-06	20:00	Friuli, Italy	6.2*	11	181	10
78-09-15		Tabas, Iran	7.4*	2	111	18
79-08-06		Coyote Lake	5.6	4	160	190
79-09-19		Valneria, Italy	5.8*	3	101	14
79-10-15		Imperial Valley	6.4*	14	60	2
80-11-23	18:34	Irpinia, Italy	6.8*	14	83	9
84-04-24		Morgan Hill	6.1	7	225	259
84-04-29		Umbria, Italy	5.6*	3	99	13
84-05-07	17:49	Lazio Abruzzo, Italy	5.5	8	206	187
86-07-08	10:09	Anza	4.1	2	11	7
87-10-01		Whittier Narrows	5.9*	12	165	15
87-11-24	13:15	Superstition Hills	6.5*	2	109	7
89-10-17		Loma Prieta	6.9*	23	171	5

* Magnitude fixed in inversion

of magnitude shown in Figure V.5-7. These data do not show a significant magnitude dependence, which supports the use of a magnitude independent stress drop for large magnitude events. The variability of the log stress drop in tectonically active regions (0.68) is approximately the same as found for the high-frequency stress parameter in ENA (0.71).

V.5.2.3 Empirical (Atkinson) Model

Atkinson (1993) developed an empirical source model for ENA earthquakes. The model is based on an extensive database that includes regional seismograph recordings, strong-motion records, teleseismic data and MMI data; it covers the magnitude range from 3 to 7.

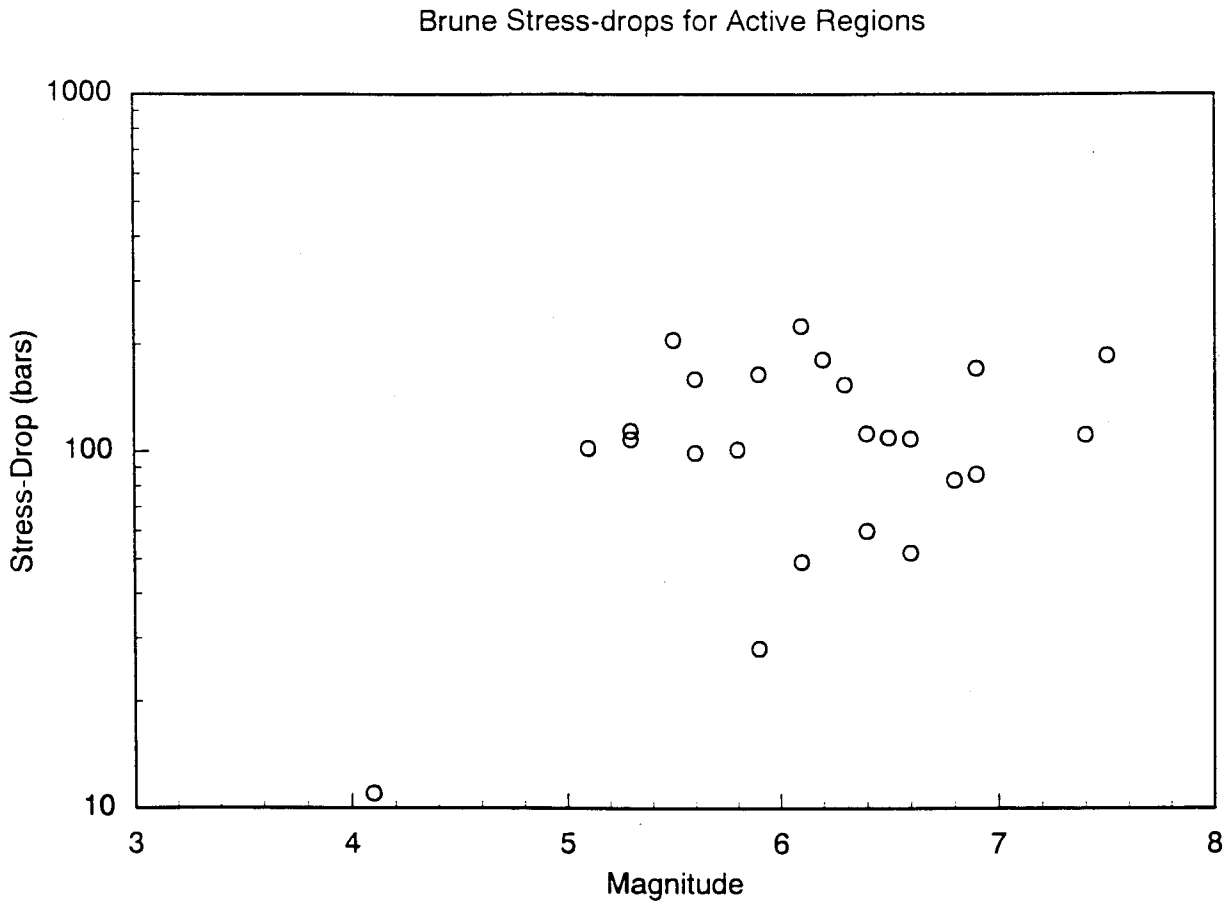

Figure V.5-7. Brune stress-drops for active regions estimated by inversion of the Fourier amplitude spectrum.

The primary data source was a set of 1200 digital seismograms, from 100 earthquakes recorded on the 30 stations of the Eastern Canada Telemetered Network (ECTN). The size of the ECTN database and its excellent distribution in distance allowed good resolution of source, path and site effects through regression analyses (Atkinson and Mereu, 1992; Boatwright, 1993). The ECTN database was supplemented at the high-magnitude end by spectral information gleaned from analyses of teleseismic data (Boatwright and Choy, 1992; Somerville et al., 1987) and from MMI data. The inclusion of MMI data was made possible by the finding that the felt area of an earthquake is highly correlated with its high-frequency spectral level at the source.

Atkinson concluded that the Brune source model does not adequately describe the shape of the source spectra of events of **M** > 5. High-frequency (5 to 10 Hz) spectral amplitudes are consistent with a Brune stress parameter of approximately 120 bars, assuming a shear-wave velocity of 3.5 km/sec in the source region (the Mid-continent velocity model, Section 5.5). Intermediate-frequency amplitudes (near 1 Hz) are matched by significantly lower stress parameters. For a shear-wave velocity of 3.5 km/sec, the equivalent Brune stress drop to match the observed 1 Hz spectral amplitudes is approximately 35 bars.

Small events (**M** < 4) are well-fit by the Brune model; however there is an apparent dependence of stress drop

on moment that is attributable to finite bandwidth effects (Boore, 1986; Atkinson, 1993; Boatwright, 1993). Thus stress drops for events of **M** < 4 that are obtained from ECTN or similar instrumentation (i.e. that cannot reliably recover amplitudes for frequencies above 10 Hz) should not be considered indicative of stress drops for larger events.

Atkinson (1993) proposed a new two-corner empirical source model based on the source spectral database. The functional form represents the addition of two Brune spectra:

$$a(f) = \frac{C f^2 M_0}{R}\left[\frac{(1-\gamma)}{1+\left(\frac{f}{f_A}\right)^2} + \frac{\gamma}{1+\left(\frac{f}{f_B}\right)^2}\right] P(f) \exp\left\{\frac{-\pi f R}{\beta Q(f)}\right\} \quad \text{(Eq. V.5-6)}$$

where f_A and f_B are the two corner frequencies given by

$$\log_{10} f_A = 2.41 - 0.533\mathbf{M}, \quad \text{(Eq. V.5-7)}$$

$$\log_{10} f_B = 1.43 - 0.188\mathbf{M}, \quad \text{(Eq. V.5-8)}$$

and γ is a fraction of the total moment given by

$$\log_{10} \gamma = 2.52 - 0.637\mathbf{M}, \quad \text{(Eq. V.5-9)}$$

(compare to Eq. 3.1). The additive form has been interpreted as follows: for events of **M**=4 (or smaller), 100% of the total moment is released by a single asperity(γ=1); this produces a simple Brune spectrum, characterized by a stress parameter of approximately 120 bars (for the Mid-continent velocity model). As magnitude increases, 'roughness' (i.e. asperities, barriers, etc.) causes enhancement of the high-frequency components of the ground motion (relative to a smooth rupture), and introduces the

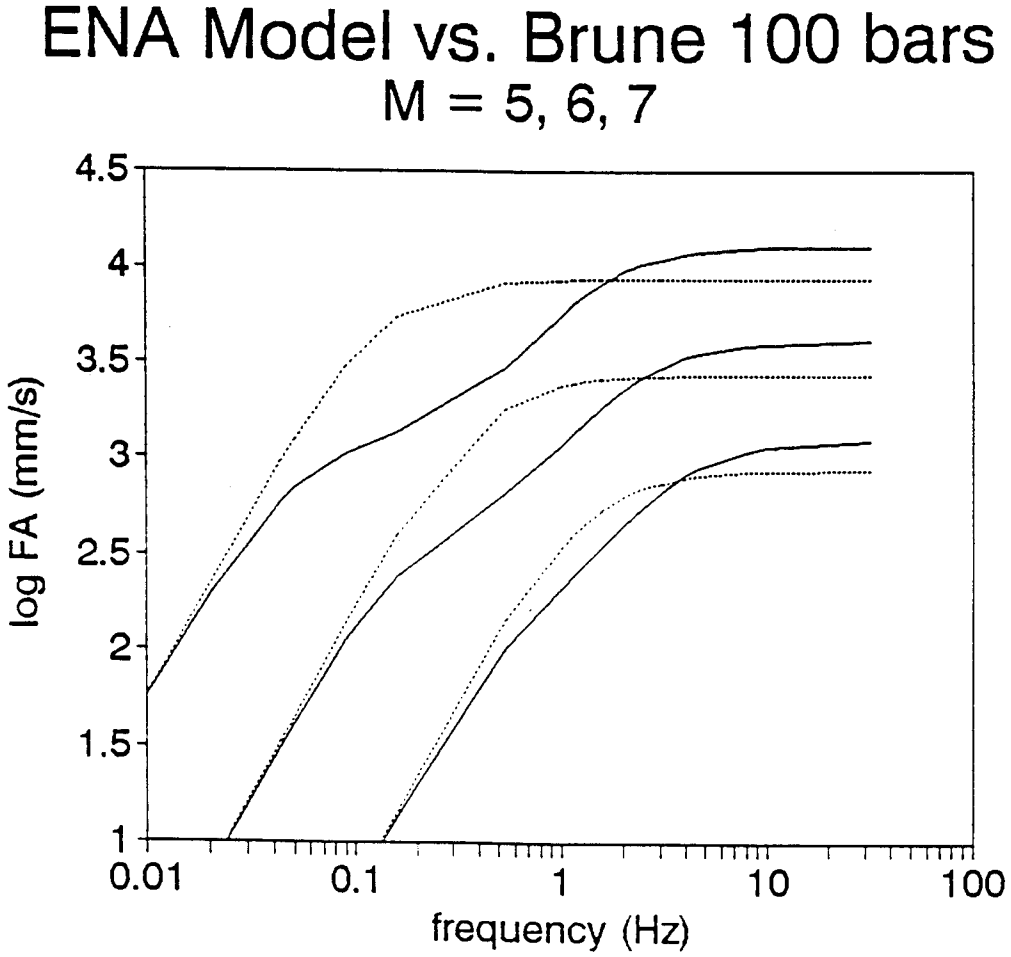

Figure V.5-8. Comparison of horizontal-component Fourier amplitude spectra (R=1 km) for the double corner Atkinson (1993) model (solid lines) with those of the 100-bar Brune model (dashed lines) for M 5, 6, and 7. From Atkinson (1993).

requirement for a second corner frequency. The Fourier amplitudes for the double-corner empirical model are compared to the Fourier amplitudes for the single-corner model (100 bars) in Figure V.5-8.

In this study, the source model proposed by Atkinson (1993) is considered in two ways. First, the estimates of the median stress parameter and its uncertainty are based on the high-frequency spectral levels from Atkinson's data set, but using the appropriate shear-wave velocities for the Mid-continent crustal model (Section V.5.2.1). Second, the sensitivity of predicted ground motion to the two-corner spectral shape is considered. It was, however, considered premature to adopt this new model which has not yet been completely reviewed and discussed by the scientific community.

V.5.2.4 Comparison of Best Single-Corner and Double-Corner Models

The simulated response spectra for the single-corner and double-corner models are compared in Figure V.5-9 for magnitude 5.5. In these figures, the double-corner model uses 1/R geometrical spreading to be consistent

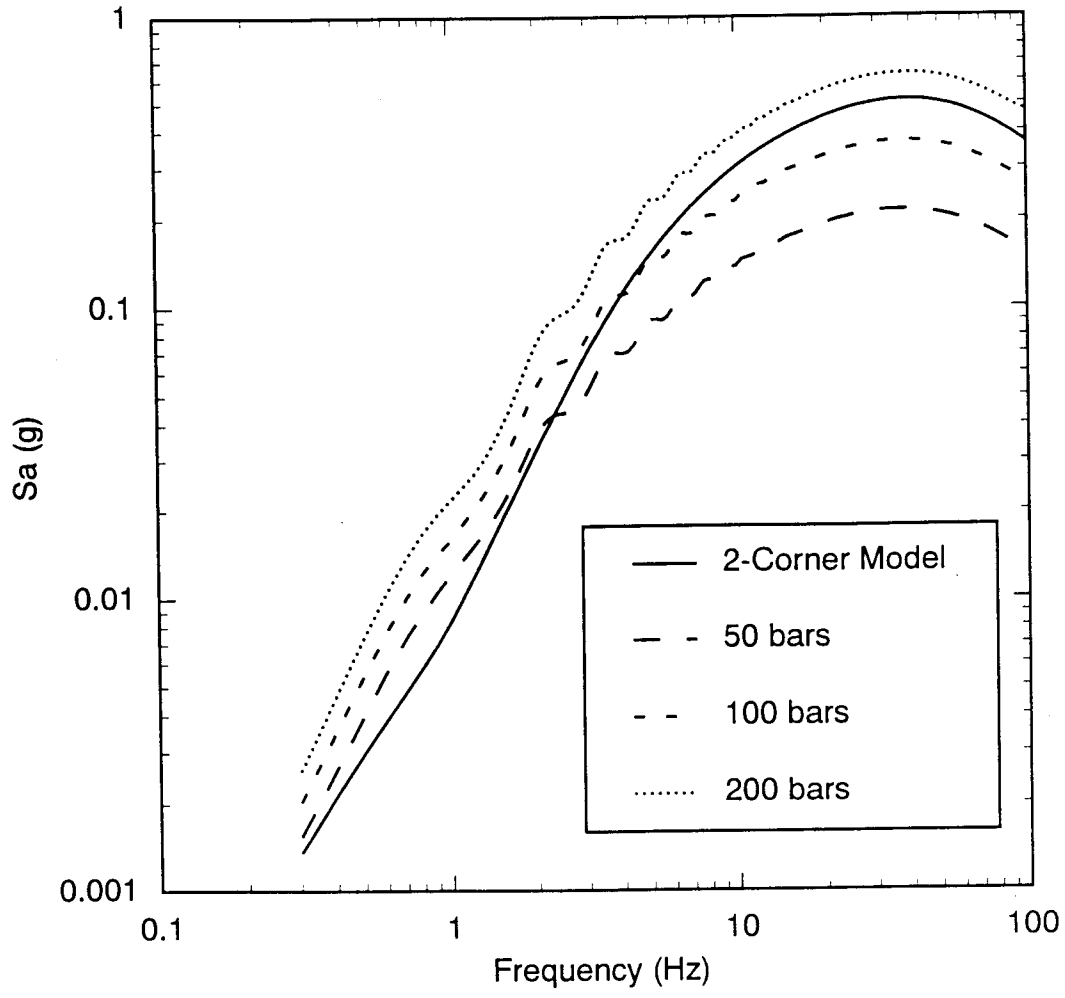

Figure V.5-9. Comparison of the response spectra for the single-corner and double corner spectral models. The double corner model uses 1/R geometrical attenuation to preserve the empirically based spectral levels, whereas the single corner model uses the Ou and Herrmann geometrical attenuation to be consistent with the application of the model in Section 9.

with the Atkinson model. Since the Atkinson model is derived empirically, we need to keep the parameters consistent in order to preserve the level of ground motion. In contrast, the single-corner model uses the Ou and Herrmann geometrical spreading factors (see Section 3). This is because the Ou and Hermann method is used in the ground motion simulations for the engineering model in Section 9. This provides a comparison of the simulations with the empirically based double-corner model.

At high frequencies, the response spectrum for the double-corner model is between the 100 bar and 200 bar stress drop response spectra for the single-corner model. At frequencies less than 3 Hz, the response spectral shape for the double-corner model departs significantly from the spectral shape for the single-corner model. At frequencies below 1 Hz, the response spectra for the double-corner model is below the 50 bar stress drop response spectrum for the single-corner model.

The single-corner model with a stress drop determined by the high frequency level will yield conservative estimates of long period response spectral in comparison to the double-corner model.

V.5.2.5 Stress Drop Model for the EUS

Both the Brune stress drop and the high frequency stress parameter can be used in the stochastic model. The high-frequency stress parameter from the Atkinson (1993) data set is used because it is a more direct measure of the high frequency level and because the Atkinson data set has many more large magnitude mainshocks than the Brune stress drop data set for SCR. In the development of the engineering model in Section 9, the stress parameter is assumed to be log normally distributed with a median of 120 bars and a standard deviation (of an estimate) of 0.7 on the natural logarithm of stress drop.

The variability of model parameters in the engineering model developed in Section 9 is divided into randomness and uncertainty. Randomness represents variability that is inherent to the parameter; uncertainty represents variability that is due to our lack of knowledge of the parameter. Therefore, randomness can be refined but not reduced, whereas uncertainty may be reduced in the future with additional information.

The stress parameter standard deviation of 0.7 is divided into uncertainty and randomness. As shown in Figure V.5-5, the mean log stress drop is unbiased for events with **M**< 6. For this magnitude range, we model the uncertainty by the standard error of the mean log stress drop which is 0.15. The remaining variability is assumed to be randomness. The randomness is calculated by subtracting the uncertainty variance from the total variance. For **M**≥6, the mean log stress drop is biased to smaller values (Figure V.5-5). The bias is large, but there are only four data points so it is not well resolved. The large but poorly resolved bias represents uncertainty whereas the scatter of the data represent randomness. The bias and standard error of the four data points for **M**≥6, are approximately equal. Therefore, we assume that the uncertainty (represented by the bias) and the randomness (represented by the standard error) are equal. The randomness and uncertainty are calculated such that the total standard error remains 0.7 (randomness = 0.5, uncertainty = 0.5). Since the bias is most apparent for **M**≥6.5, this randomness and uncertainty are used for **M**≥6.5 and linear interpolation on the variance is used to give a smooth transition between **M**=6 and **M**=6.5. The resulting randomness and uncertainty are given by

Randomness:

$$\begin{cases} 0.684 & \mathbf{M} \le 6.0 \\ \sqrt{(0.684)^2 - 0.436(M-6)} & 6.0 < \mathbf{M} < 6.5 \\ 0.50 & \mathbf{M} \ge 6.5 \end{cases} \qquad \text{(Eq. V.5-10)}$$

Uncertainty:

$$\begin{cases} 0.15 & \mathbf{M} \le 6.0 \\ \sqrt{(0.15)^2 + 0.455(M-6)} & 6.0 < \mathbf{M} < 6.5 \\ 0.50 & \mathbf{M} \ge 6.5 \end{cases} \qquad \text{(Eq. V.5-11)}$$

V.5.3 Extended Source Effect

The simulation procedure described in Section 3.2 uses an equivalent point source distance to define the distance from large magnitude events. This distance corresponds to the distance to the closest point on the rupture plane at the depth of the main slip (called the asperity). For large events with extended sources, this distance does not necessarily represent hypocentral distance. When all possible azimuths are considered, the family of equivalent point sources defines a line or the fault plane at the depth of the asperity.

In Section 5.2, depth distributions for events in ENA are developed. These depth distributions are for hypocentral depth, whereas the depth used in the point source model is asperity depth. In order to use these focal depth distributions with the simulation procedure, we need a conversion from hypocentral depth to asperity depth to account for the extended source effect. In addition, we need to consider the spatial extent of the source in terms of the probability that a large magnitude event will occur at shallow focal depths.

These two effects depend on the distribution of hypocenter depths and asperity depths for large magnitude events. For most large events, we do not have reliable estimates of the distribution of slip and hence the depth of the asperity; however, for many recent large events, slip distribution information is available based on inversions of strong-motion data. A set of 11 large events with estimated slip distributions is listed in Table V.5-4. The hypocenter and asperity depths are listed as a fraction of the down-dip width of the fault rupture. Histograms of the hypocenter and asperity depths are shown in Figure V.5-10. The median hypocenter location is 12% further down-dip than the median asperity location. For fault dips uniformly distributed between 30 and 90 degrees, the median hypocenter depth is deeper than the median asperity depth by approximately 10% of the rupture width.

To compute the difference in hypocenter depth and asperity depth using the analysis above requires an estimate of the rupture width. An empirical relation between rupture width and moment magnitude is derived using the Wells and Coppersmith (1992) data set. The down-dip rupture width (width in the fault plane), w, is given by

$$\ln w(km) = -2.67 + 0.79\mathbf{M} \qquad \text{(Eq. V.5-12)}$$

for dip-slip and oblique-slip events with $\mathbf{M} \leq 8$ and strike-slip events with $\mathbf{M} \leq 7$. For strike-slip events with $\mathbf{M} > 7$, the median w is constant at 17.5 km (Figure V.5-11). The width-magnitude relation is approximately log normally distributed with a standard error of 0.75 natural log units. The resulting mean hypocentral depth for a given asperity depth is

$$h_{hypo} = h_{asperity} + 0.1\exp(-2.67 + 0.79\mathbf{M}) \qquad \text{(Eq. V.5-13)}$$

This relation is plotted in Figure V.5-12. The complete relation between hypocentral depth and asperity depth requires a probability density function; however for ease

Table V.5-4

Large Magnitude Events with Estimated Slip Distributions

Event	M	Asperity Depth(%)	Hypocenter Depth(%)	Reference
1971 San Fernando	6.5	0.46	0.72	Heaton, 1982
1976 Tabas	7.4	0.42	0.30	Hartzell & Mendoza, 1991
1979 Coyote Lake	5.9	0.52	0.67	Liu & Helmberger, 1983
1979 Imperial Valley	6.5	0.59	0.85	Hartzell & Heaton, 1983
1984 Morgan Hill	6.2	0.59	0.71	Hartzell & Heaton, 1986
1984 Borah Peak	7.3	0.74	0.76	Hartzell & Mendoza, 1988
1985 Nahanni	6.8	0.60	0.46	Wald, 1991
1986 N. Palm Springs	6.0	0.68	0.76	Hartzell, 1989
1987 Superstition Hills	6.6	0.55	0.68	Wald et al., 1990
1987 Whittier	6.0	0.67	0.50	Hartzell & Iida, 1990
1989 Loma Prieta	7.0	0.46	0.80	Wald et al., 1990

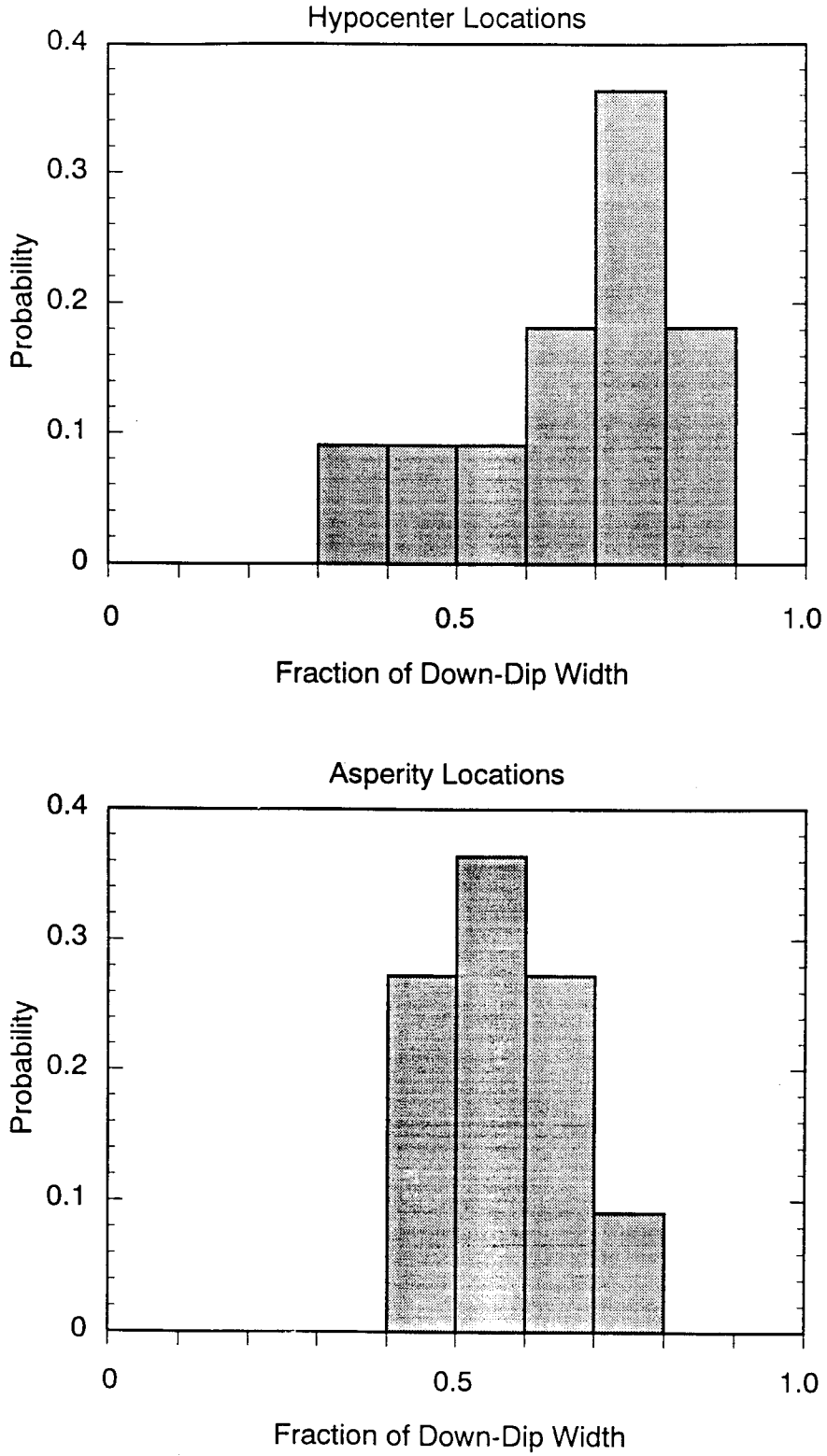

Figure V.5-10. Discrete probability distributions for the hypocenter and asperity locations in terms of the fraction of the down-dip width. These probabilities are based on slip models estimated for 11 large magnitude events.

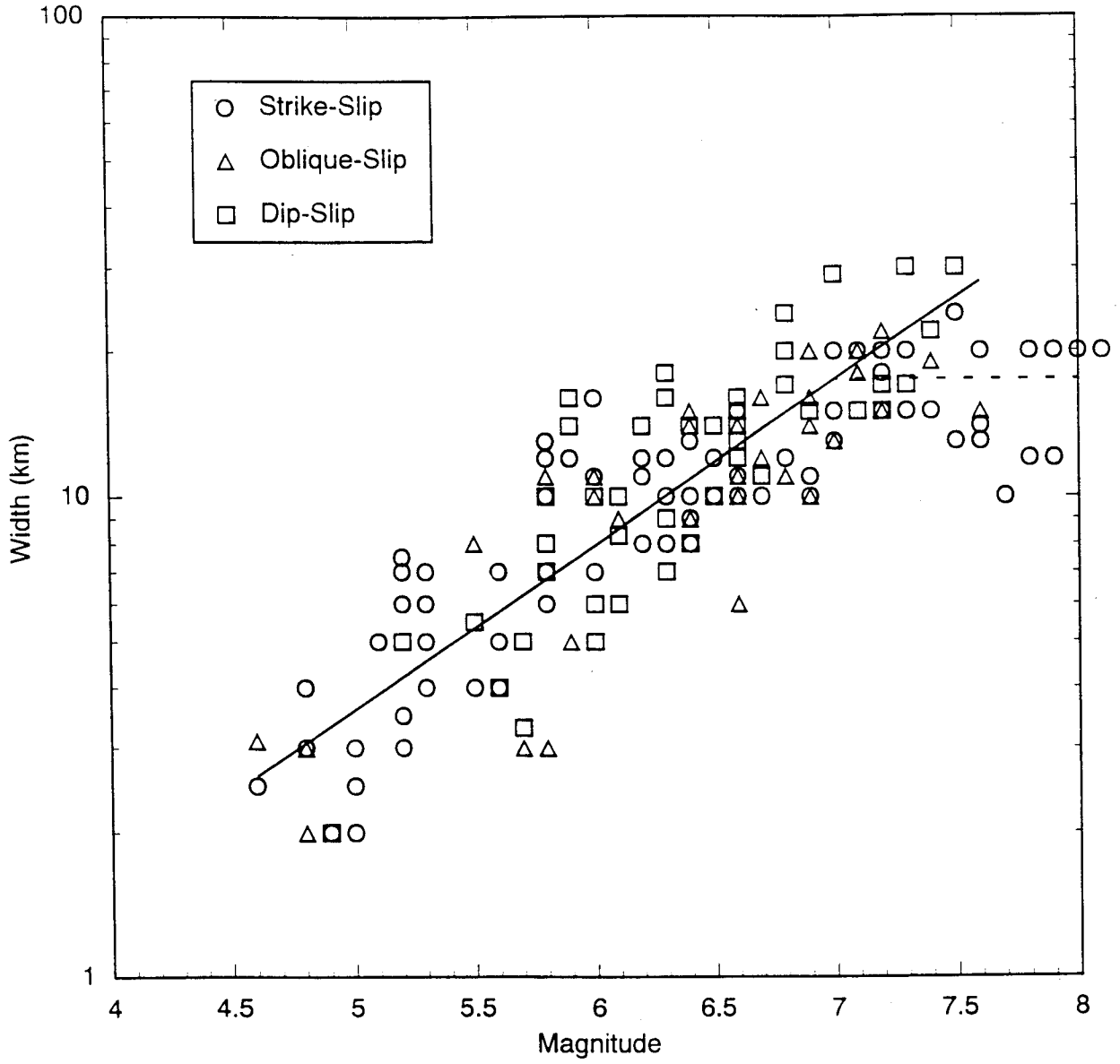

Figure V.5-11. Empirical relation between fault rupture width and moment magnitude. Data are from Wells and Coppersmith (1992).

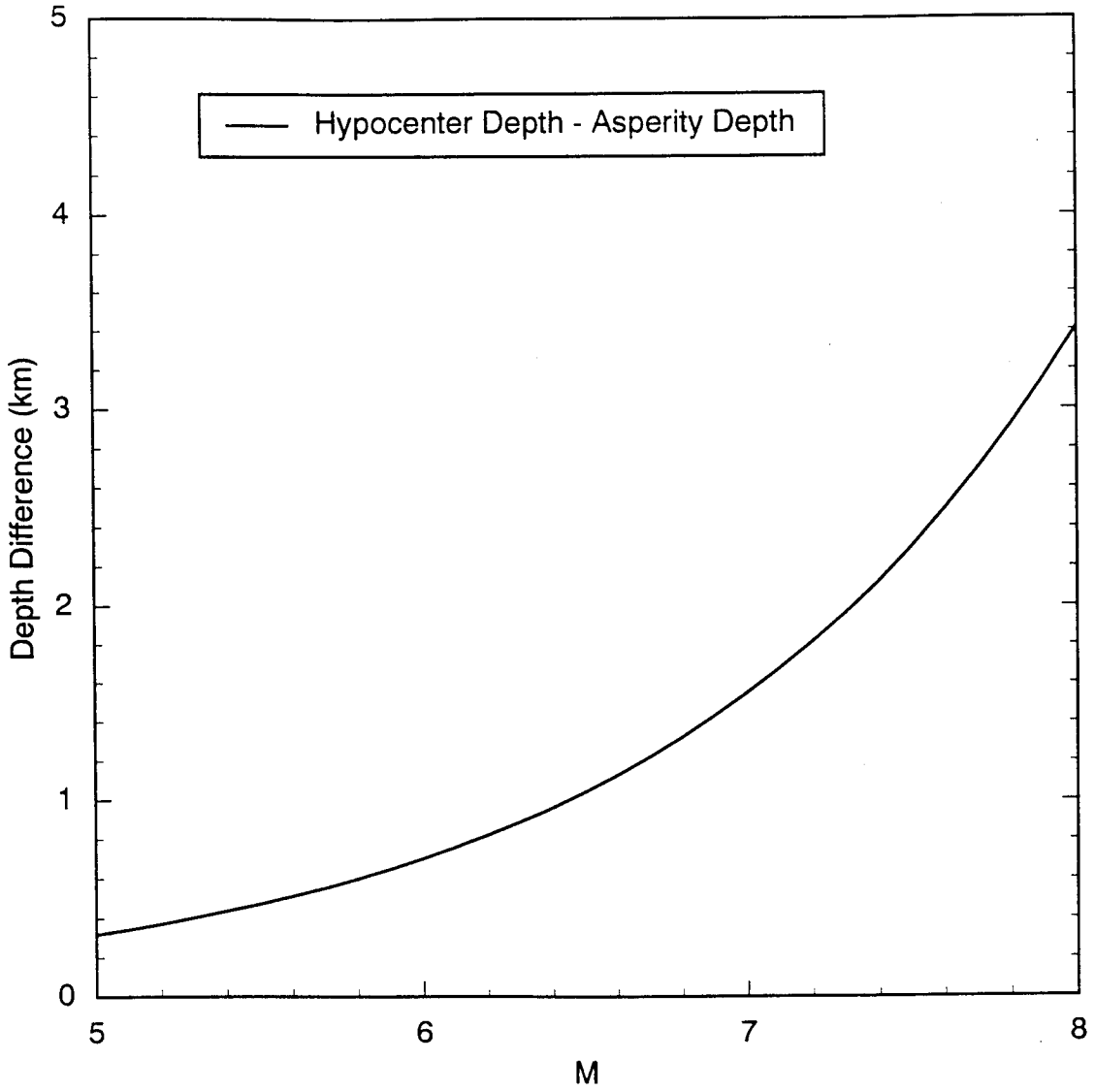

Figure V.5-12. Difference in median hypocenter depth and median asperity depth as a function of magnitude as predicted by Eq. V.5-11.

of application in the regression analysis in Section 9, only the mean hypocentral depth is used for the given asperity depth.

The second extended-source effect results from geometrical constraints on the fault rupture dimension. The geometrical constraint is that the rupture width be contained between 0 and 35 km depth. (The 35 km maximum depth is justified in Section 5.2.) The depths of the top and bottom of the rupture are given by

$$z_{top}(h,\theta,\varepsilon,w,\mathbf{M}) = h - \sin(\theta)\, w(\mathbf{M})\, \varepsilon \quad \text{(Eq. V.5-14)}$$

and

$$z_{bottom}(h,\theta,\varepsilon,w,\mathbf{M}) = h + \sin(\theta)\, w(\mathbf{M})\, (1-\varepsilon) \quad \text{(Eq. V.5-15)}$$

where h is the hypocenter depth, θ is the fault dip, and ε is the fraction of the down-dip width of the hypocenter location. The probability that a given magnitude and

hypocenter depth pair lead to a realizable solution (i.e. meet the geometrical constraint) is given by

$$P(\text{realizable} \mid h,M) = \sum_{i=1}^{n_\varepsilon} \int_{\theta=30}^{90} \int_{w=0}^{\infty} H(z_{top}(h,\theta,\varepsilon_i,w,\mathbf{M})) \, H(35\text{-}z_{bottom}(h,\theta,\varepsilon_i,w,\mathbf{M})) \, f_w(w,\mathbf{M}) \, P(\varepsilon_i) \, dw \, d\theta$$

(Eq. V.5-16)

where H is the heaviside function, f_w is the probability density function of the rupture width from Eq. V.5-13 (log normal), $P(\varepsilon_i)$ is the probability of ε_i (treated as a discrete variable), and n_ε is the number of discrete ε considered. $P(\varepsilon_i)$ is computed from the distribution of hypocenter locations shown in Figure V.5-10. The probabilities for Eq. V.5-16 are listed in Table V.5-5 and are plotted in Figure V.5-13 for magnitudes 5, 6, 7, and 8.

In Section 5.2, discrete empirical hypocenter depth distributions applicable for the ENA are developed. If the probability of the hypocenter depth distribution is given by $P(h_j)$, then the joint probability of a hypocenter and a realizable solution for a given magnitude is given by

$$P(h_j,\text{realizable} \mid \mathbf{M}) = P(\text{realizable} \mid h_j,\mathbf{M}) \, P(h_j)$$

(Eq. V.5-17)

To preserve the total number events at each magnitude, this probability needs to be normalized such that the sum of the probabilities over all of the hypocenter depths is unity. This normalization leads to the following normalized probability

$$\tilde{P}(h_j,\text{realizable} \mid \mathbf{M}) = \frac{P(\text{realizable} \mid h_j,\mathbf{M}) \, P(h_j)}{\sum_{j=1}^{n_h} P(\text{realizable} \mid h_j,\mathbf{M}) \, P(h_j)}$$

(Eq. V.5-18)

where n_h is the number of discrete hypocenter depths considered.

V.5.3.1 Example

An example probability distribution for hypocenters is shown in Figure V.5-14a. The normalized probability for realizable depth distributions, P, for a magnitude 7 event is shown in Figure V.5-14b. The number of shallow hypocentral depth events are significantly reduced. Based on Eq. V.5-13, the corresponding asperity depth distribution for a magnitude 7 event based on Eq. V.5-13 would be shifted to shallower depths by 1.7 km.

Table V.5-5

Probability of Realizable Hypocentral Depth and Magnitude Pairs

	Hypocentral Depth					
M	**5 km**	**10 km**	**15 km**	**20 km**	**25 km**	**30 km**
5.0	1.00	1.00	1.00	1.00	1.00	1.00
5.5	0.99	1.00	1.00	1.00	1.00	1.00
6.0	0.92	1.00	1.00	1.00	1.00	0.97
6.5	0.77	0.98	1.00	1.00	1.00	0.88
7.0	0.56	0.90	0.98	1.00	0.96	0.70
7.5	0.40	0.72	0.90	0.94	0.84	0.51
8.0	0.29	0.51	0.72	0.78	0.64	0.36

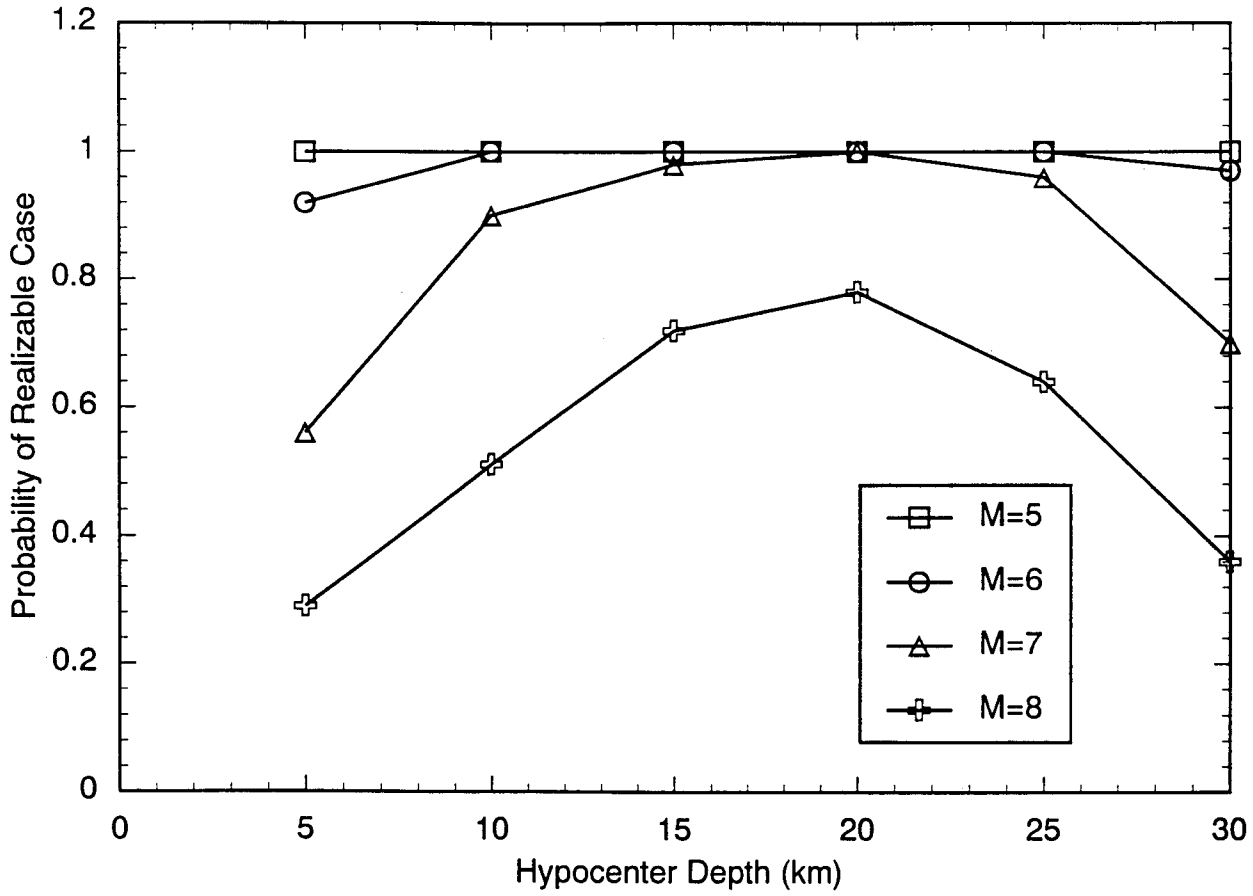

Figure V.5-13. Probability that a hypocenter-magnitude pair is physically realizable due to geometrical constraints on the rupture dimension (Eq. V.5-14). The rupture is restricted to the depth range of 0 to 35 km.

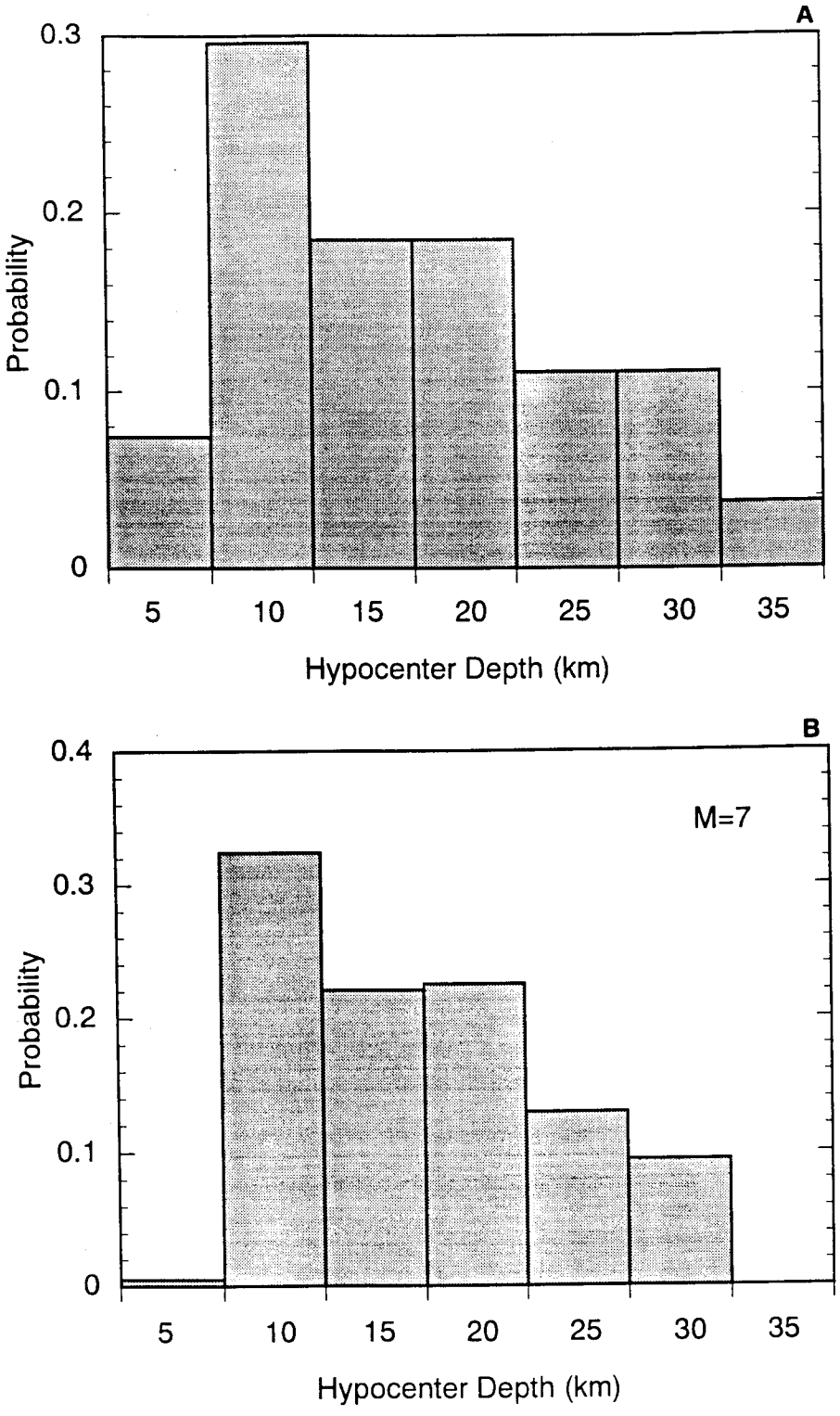

Figure V.5-14. (A) Example hypocenter depth distribution from earthquake catalogs for events with M>5. (B) Resulting hypocenter depth probability distribution after accounting for the geometrical constraints on the rupture dimension (Eq. V.5-16).

References

Atkinson, G. M. (1984). Attenuation of strong ground motion in Canada from a random vibration approach, *Bull. Seism. Soc. Am.*, 74, 2629–2653.

Atkinson, G. M. (1993). Earthquake source spectra in Eastern North America, submitted to *Bull. Seism. Soc. Am.*

Atkinson, G. M. and R. Mereu (1992). The shape of ground motion attenuation curves in southeastern Canada, *Bull. Seism. Soc. Am.*, 82, in press.

Boatwright, J. (1993). Regional propagation characteristics and source parameters of earthquakes in eastern North America. *Bull. Seism. Soc. Am.*, submitted.

Boatwright, J. and G. Choy (1992). Acceleration source spectra anticipated for large earthquakes in Northeastern North America, *Bull. Seism. Soc. Am.*, 81, 1783–1812.

Boore, D. M. (1983). Stochastic simulation of high-frequency ground motions based on seismological models of the radiated spectra, *Bull. Seism. Soc. Am.*, 73, 1865–1894.

Boore, D. M. (1986). The effect of finite bandwidth of seismic scaling relationships, Proc. 6th Ewing Symp., *Am. Geophys. Union*, Geophysical Monograph, 37.

Boore, D. M. and G. M. Atkinson (1987). Stochastic prediction of ground motion and spectra response parameters at hard-rock sites in eastern North America, *Bull. Seism. Soc. Am.*, 77, 440–467.

EPRI (1986). Seismic hazard methodology for the Central and Eastern U.S., EPRI Report NP-4726A.

Hanks, T. C. and D. M. Boore (1984). Moment-magnitude relations in theory and practice, *J. Geophys. Res.*, 89, 6229–6235.

Hanks, T. C. and H. Kanamori (1979). A moment magnitude scale, *J. Geophys. Res.*, 84, 2348–2350.

Hartzell, S. H. (1989). Comparison of seismic waveform inversion techniques for the rupture history of a finite fault: application to the 1986 North Palm Springs, California, earthquake, *J. Geophys. Res.*, 94, 7515–7534.

Hartzell, S. H. and T. H. Heaton (1983). Inversions of strong ground motion and Teleseismic waveform data for the fault rupture history of the 1979 Imperial Valley, California, earthquake, *J. Geophys. Res.*, 94, 7515–7534.

Hartzell, S. H. and T. H. Heaton (1986). Rupture history of the 1984 Morgan Hill, California, earthquake from the inversion of strong motion records, *Bull. Seism. Soc. Am.*, 76, 649–674.

Hartzell, S. H. and M. Iida (1990). Source complexity of the 1987 Whittier Narrows, California, earthquake from the inversion of strong motion records, *J. Geophys. Res.*, 95, 12475–12485.

Hartzell, S. H. and C. Mendoza (1991). Application of an iterative least-squares waveform inversion of strong motion and teleseismic records to the 1978 Tabas, Iran, earthquake, *Bull. Seism. Soc. Am.*, 81, 305–331.

Heaton, T. H. (1982). Evidence for and implications of self-healing pulses of slip in earthquake rupture, Phys. Earth Planet. *Interiors*, 64, 1–20.

Herrmann, R. B. and O. W. Nuttli (1980). Strong motion investigations in the Central United States. *Proceedings: Seventh World Conference on Earthquake Engineering*, Istanbul, II, 533–536.

Liu, H. L. and D. V. Helmberger (1983). The near-source ground motion of the 6 August 1979 Coyote Lake, California, earthquake, *Bull. Seism. Soc. Am.*, 73, 21–218.

LLNL (1989). Seismic hazard characterization of 69 plant sites east of the Rocky Mountains: methodology, input data and comparisons to previous results for ten test sites, NRC Report NUREG/CR5250, UCID-21517.

Luh, P. C. (1977). A scheme for expressing instrumental responses parametrically, *Bull. Seism. Soc. Am.*, 67, 950–957.

McGuire et al. (1988). Engineering model of earthquake ground motion for eastern North America, EPRI Report NP-6074.

Mendoza, C. and S. H. Hartzell (1988). Inversion for slip distribution using GDSN P waves: North Palm Springs, Borah Peak, and Michoacan earthquakes, *Bull. Seism. Soc. Am.*, 78, 1092–1111.

Nuttli, O. W. (1973). Seismic wave attenuation and magnitude relations for eastern North America, *J. Geophys. Res.*, 78, 876–885.

Nuttli. O. W. (1983). Average seismic source parameter relations for mid-plate earthquakes, *Bull. Seism. Soc. Am.*, 73, 519–535.

Silva, W. J., and C. L. Stark (1992). Source, path, and site ground motion model for the 1989 M 6.9 Loma Prieta earthquake, CDMG draft final report.

Silva, W. J. (1991). Global characteristics and site geometry, Proceedings: NSF/EPRI Workshop on Dynamic Soil Properties and Site Characterization, Electric Power Res. Inst., EPRI NP-7337.

Somerville, P. G., J. P. McLaren, L. V. LeFevre, R. W. Burger, and D. V. Helmberger (1987). Comparison of source scaling relations of eastern and western North American earthquakes, *Bull. Seism. Soc. Am.*, 77, 322–346.

Somerville, P. G. (1986). *Source scaling relations of eastern North American earthquakes*, EPRI Report NP-4789.

Toro, G. R. (1988). *Prediction of earthquake ground motions in eastern North America using simple models of source spectrum and wave propagation*, EPRI Report NP-5577.

Toro, G. R. and R. McGuire (1987). An investigation into earthquake ground motion characteristics in eastern North America, *Bull. Seism. Soc. Am.*, 77, 468–489.

Wald, D. J., D. V. Helmberger and T. H. Heaton (1991). Rupture model of the 1989 Loma Prieta earthquake from the inversion of strong motion and broadband teleseismic data, *Bull. Seism. Soc. Am.*, 81, 1540–1572.

Wald, D. J., D. V. Helmberger, and S. H. Hartzell (1990). Rupture process of the 1987 Superstition Hills earthquake from the inversion of strong-motion data, *Bull. Seism. Soc. Am.*, 80, 1079–1098.

Wells, D. L. and K. J. Copersmith (1992). Updated empirical relationships among magnitude, rupture length, rupture area, and surface displacement, Submitted to Bull. Seism. Soc. Am.

About EPRI

EPRI creates science and technology solutions for the global energy and energy services industry. U.S. electric utilities established the Electric Power Research Institute in 1973 as a nonprofit research consortium for the benefit of utility members, their customers, and society. Now known simply as EPRI, the company provides a wide range of innovative products and services to more than 1000 energy-related organizations in 40 countries. EPRI's multidisciplinary team of scientists and engineers draws on a worldwide network of technical and business expertise to help solve today's toughest energy and environmental problems.

EPRI. Electrify the World

Printed on recycled paper in the United States of America

EPRI • 3412 Hillview Avenue, Palo Alto, California 94304 • PO Box 10412, Palo Alto, California 94303 • USA
800.313.3774 • 650.855.2121 • askepri@epri.com • www.epri.com